PCCP

Dyads with Tunable Near-Infrared Donor-Acceptor Excited-State Energy Gaps: Molecular Design and Förster Analysis for Ultrafast Energy Transfer

Journal:	*Physical Chemistry Chemical Physics*
Manuscript ID	CP-ART-10-2022-004689.R2
Article Type:	Paper
Date Submitted by the Author:	30-Nov-2022
Complete List of Authors:	Jing, Haoyu; NC State University, Chemistry Magdaong, Nikki Cecil; Washington University in St Louis, Chemistry Diers, James; University of California Riverside Kirmaier, Christine; Washington University in St Louis Bocian, David; University of California Riverside, Chemistry Holten, Dewey; Washington University in St Louis Lindsey, Jonathan; NC State University

Dyads with Tunable Near-Infrared Donor–Acceptor Excited-State Energy Gaps: Molecular Design and Förster Analysis for Ultrafast Energy Transfer

Haoyu Jing[a], Nikki Cecil M. Magdaong[b], James R. Diers[c], Christine Kirmaier[b], David F. Bocian[c,*], Dewey Holten[b,*] and Jonathan S. Lindsey[a,*]

[a]Department of Chemistry
North Carolina State University
Raleigh, North Carolina 27695-8204
e-mail: jlindsey@ncsu.edu
Tel: +1-919-515-6406

[b]Department of Chemistry
Washington University
St. Louis, Missouri 63130-4889
e-mail: holten@wustl.edu
Tel: +1-314-935-6502

[c]Department of Chemistry
University of California, Riverside
Riverside, California 92521-0403
e-mail: david.bocian@ucr.edu
Tel: +1-951-827-3660

Abstract

Bacteriochlorophylls, nature's near-infrared absorbers, play an essential role in energy transfer in natural photosynthetic antennas and reaction centers. To probe energy-transfer processes akin to those in photosynthetic systems, nine synthetic bacteriochlorin–bacteriochlorin dyads have been prepared wherein the constituent pigments are joined at the *meso*-positions by a phenylethyne linker. The phenylethyne linker is an unsymmetric auxochrome, which differentially shifts the excited-state energies of the phenyl- or ethynyl-attached bacteriochlorin constituents in the dyad. Molecular designs utilized known effects of macrocycle substituents to engineer bacteriochlorins with $S_0 \rightarrow S_1$ (Q_y) transitions spanning 725 – 788 nm. The design-predicted donor–acceptor excited-state energy gaps in the dyads agree well with those obtained from time dependent density

functional theory calculations and with the measured range of 197 – 1089 cm^{-1}. Similar trends with donor–acceptor excited-state energy gaps are found for (1) the measured ultrafast energy-transfer rates of $(0.3\ ps)^{-1} – (1.7\ ps)^{-1}$, (2) the spectral overlap integral (J) in Förster energy-transfer theory, and (3) donor–acceptor electronic mixing manifested in the natural transition orbitals for the $S_0 \rightarrow S_1$ transition. Subtle outcomes include the near orthogonal orientation of the π-planes of the bacteriochlorin macrocycles, and the substituent-induced shift in transition-dipole moment from the typical coincidence with the NH–NH axis; the two features together afforded the Förster orientation term κ^2 ranging from 0.55–1.53 across the nine dyads, a value supportive of efficient excited-state energy transfer. The molecular design and collective insights on the dyads are valuable for studies relevant to artificial photosynthesis and other processes requiring ultrafast energy transfer.

Introduction

The flow of excited-state energy from one molecule to another underpins a wide variety of phenomena of importance across diverse disciplines. In photosynthesis, antenna complexes serve to absorb sunlight and funnel excited-state energy, among a collection of pigments, to the reaction centers where charge separation occurs.[1] In biochemical assays, absorption of light by a donor, excited-state energy transfer from the donor to an acceptor, and ensuing fluorescence emission of the latter enables detection of molecular proximity of the two constituents.[2] In clinical diagnostics, a collection of donor–acceptor molecules comprised of a common donor but distinct acceptors enables single-wavelength irradiation to be employed yet elicit distinct wavelengths (i.e., "colors") of emission.[3]

A mechanism for excited-state energy transfer was first described by Förster in the mid-twentieth century.[4-7] The mechanism entails the through-space resonant coupling of the transition-dipole moment (TDM) of the donor and the TDM of the acceptor.[8-10] The Förster mechanism,

which has been referred to by almost 20 names,[11] has been found to be valid for a wide variety of molecular constructs ranging from freely diffusing donors and acceptors in solution to rigidly organized 3-dimensional assemblies of large collections of interacting pigments.[12-28] In recent years, electronic-vibrational coherences have been observed upon examination by ultrafast 2-dimensional spectroscopy of photosynthetic complexes and model systems.[29-46] Such coherences emerge when the donor–acceptor excited-state energy-transfer gap is resonant with a vibration in one of the constituents. Despite the observation of such coherences, a critical unknown has been the contribution of the coherence to the rate of excited-state energy transfer beyond that expected solely on the basis of incoherent, Förster energy transfer.[47]

To address this critical lacuna, we recently prepared a set of nine dyads wherein each dyad is comprised of a bacteriochlorin donor, a bacteriochlorin acceptor, and phenylethynyl linker joining the two macrocycles. The dyads are shown in Chart 1. Each bacteriochlorin contains a π-chromophore resembling that of the native bacteriochlorophyll *a* of anoxygenic photosynthesis.[48,49] The bacteriochlorin absorbs strongly in the near-ultraviolet (NUV) and in the near-infrared (NIR) spectral regions. The dyads were designed to encompass a range of excited-state energy gaps given by the difference in the position of fluorescence emission of the donor and long-wavelength absorption of the acceptor. The energy levels were tuned by strategic placement of substituents on the two bacteriochlorins, giving a resulting energy range from ~200 – 1100 cm^{-1}. Examination of the nine dyads found that the rate of excited-state energy transfer was the same as expectation in the standard Förster mechanism within a factor of two regardless of the likely presence of vibrational-electronic resonances.[47]

In this paper, we provide a full account of the molecular design and synthesis of the bacteriochlorin dyads, which have not been previously published. The molecular design relies on the use of substituents to tune the long-wavelength absorption band of the bacteriochlorins, with

particular choice of substituents done in concert with knowledge concerning the limitations of the synthetic methodology of bacteriochlorins. Some substituents were chosen for double duty, providing wavelength tuning and facilitating chromatographic separation following chemical installation. We also provide a full account of the Förster treatment of the bacteriochlorin dyads. The in depth presentation is essential for a number of reasons. Although Förster theory is widely employed, the means of obtaining some of the input parameters are often unclear, and pitfalls exist that are not always obvious.[10,28] Generic input values are often utilized that are not applicable when the donor and acceptor are covalently linked. In the present case, additional subtle features arise from the unusual and unexpected, energy-minimum orthogonal orientation of the respective macrocycles. Finally, we describe calculations via (1) density functional theory (DFT) to obtain the energies and electron-density distributions of the frontier molecular orbitals (MOs) of the benchmark donor monomers, benchmark acceptor monomers, and the dyads, and (2) time-dependent DFT (TDDFT) calculations to obtain spectral and excited-state properties for the monomers and dyads. The latter gives rise to the electronic compositions of the excited states responsible for the visible and NIR absorption spectra. The natural transition orbitals (NTOs) were also obtained, which help visualize the electron-density changes that occur in making a transition from the ground state to a given excited state. Taken together, the results provide a clear understanding of the rational design of a set of dyads with wavelength-tunable features in the relatively unexplored NIR spectral region.

Results and discussion

1. Molecular design

The goal of this work was to create a family of bacteriochlorin dyads wherein each shares a common architecture yet the dyads collectively exhibit a finely tuned range of donor–acceptor

excited-state energy differences. A key design constraint was to achieve the energy tuning with minimalist, sparsely substituted macrocycles so as to limit the structural complexity and consequent vibrational richness.[50] These constraints affect the choice of the linker joining the two macrocycles and the nature of the substituents on the respective macrocycles. We consider both in turn. Each bacteriochlorin contains a gem-dimethyl group in the pyrroline ring, which precludes adventitious dehydrogenation characteristic of the unsubstituted pyrroline systems.[51]

A. Known substituent effects in bacteriochlorins. Extensive studies have shown that the long-wavelength (Q_y) band of a free base bacteriochlorin can be tuned from 713 nm to 1033 nm.[52] However, achieving such large tuning requires substantial derivatization of the macrocycle; in particular, the very long wavelength absorption is obtained with annulation of the macrocycle. A more limited (but still substantial) tuning has been achieved by introduction of substituents at the 3- and 13-positions, which are coincident with the y axis of the molecule.[53] A list of such substituents is provided in Table 1.

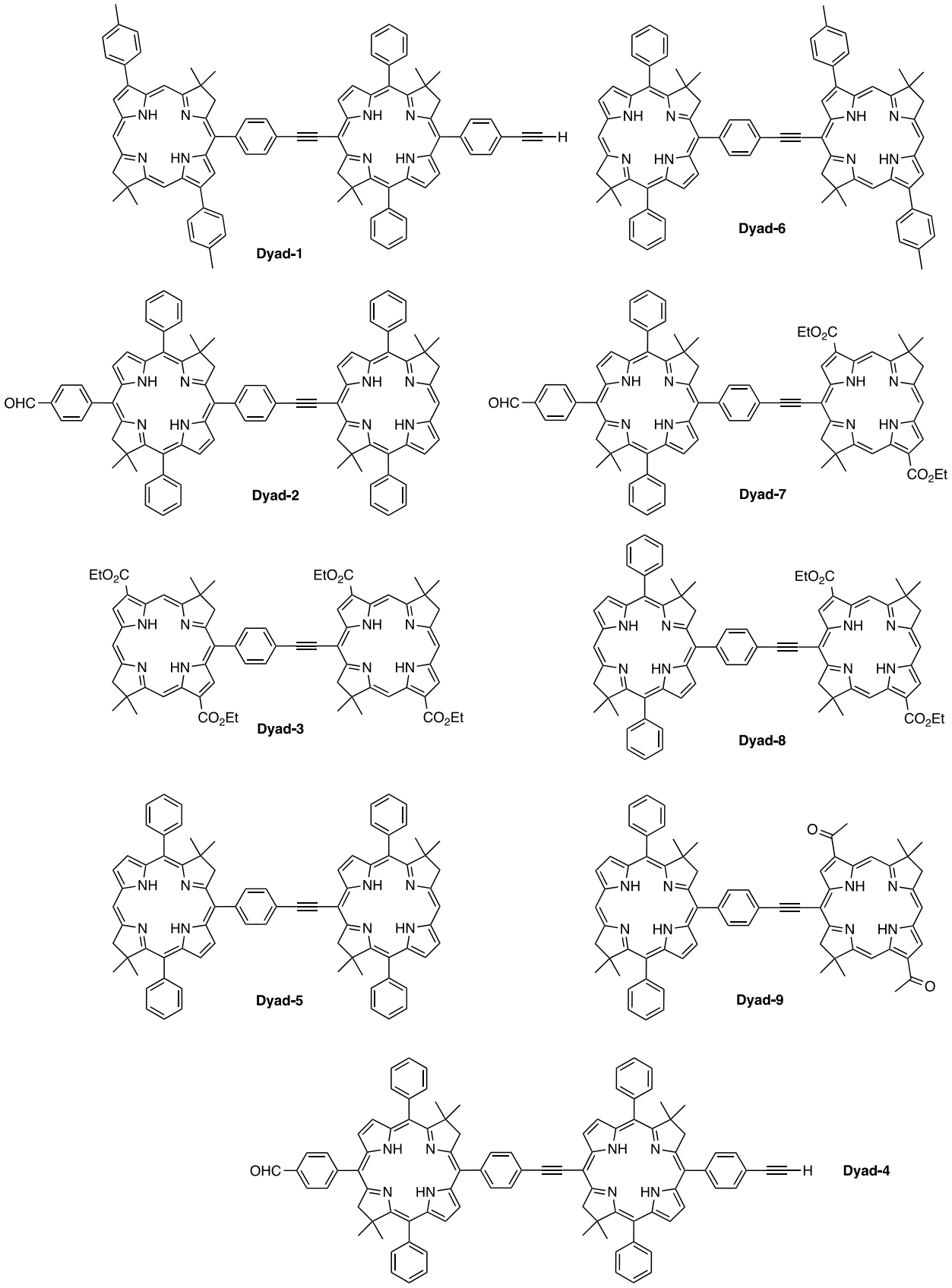

Chart 1. Nine bacteriochlorin dyads.

Table 1. Wavelength tuning with 3- and 13-substitution of bacteriochlorins.

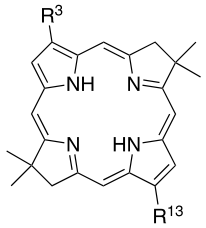

cmpd	$R^{3,13}$	Q_y (nm)	$\Delta\lambda$ (nm)	$\Delta\nu$ (cm^{-1})
A	H–	713	0	--
B	phenyl–	736	23	438
C	cyano–	749	36	674
D	vinyl–	750	37	692
E	MeO_2C–	754	41	763
F	phenylethynyl–	763	50	919
G	acetyl–	768	55	1004
H	formyl–	771	58	1055

The linker joining the two bacteriochlorins is not expected to be benign with regards to wavelength tuning. Initially we sought the *p*-phenylene linker, which would provide a very compact architecture with the bacteriochlorins in close proximity, but encountered substantial synthetic challenges. Indeed, *p*-phenylene-linked bacteriochlorin dyads have been studied computationally[54] but have not yet been accessed via synthesis, although symmetric dimers[55] and dyads[56,57] have recently been prepared that are built upon the gem-dimethyl-substituted building blocks; earlier bacteriochlorin dyads have been built from naturally derived macrocycles.[58] The dearth can be compared with the vast collection of extant *p*-phenylene-linked porphyrins.[59] We also considered the 1,4-diphenylethyne linker, but regarded the distance between the two bacteriochlorins as too great for the planned energy-transfer studies. Ultimately, consideration of both desired photophysical properties and available synthetic methodology led to use of the phenylethyne linker. The phenylethyne linker is unsymmetrical in that the bacteriochlorin attached to the phenyl versus ethynyl moiety is expected to undergo a respective small versus large spectral

shift of the Q_y band. Examples are provided in Figure 1. The 10,20-diphenylbacteriochlorin **I** exhibits the Q_y band at 721 nm, to be compared with the fully unsubstituted, core bacteriochlorin (**A**, 713 nm). The installation of an aryl group – here either a *p*-formylphenyl group (**II**) or a *p*-ethynylphenyl group (**III**) – gives the Q_y band at 725 nm. On the other hand, the phenylethynyl group at a meso (i.e., 5-, 10-, 15-, or 20-) position of the bacteriochlorin imparts a bathochromic shift of the Q_y band of ~22 nm, as discerned upon examination of bacteriochlorins **IV** and **V**.[60] The contrast between the bathochromic shift of the *p*-ethynylphenyl group (4 nm) versus the phenylethynyl unit (22 nm) is substantial. Note also the position-dependent shift imparted by phenyl groups: two aryl units at the β-positions (**C**) cause a 23 nm Q_y band shift but only 8 nm if at the meso-positions (**B**).

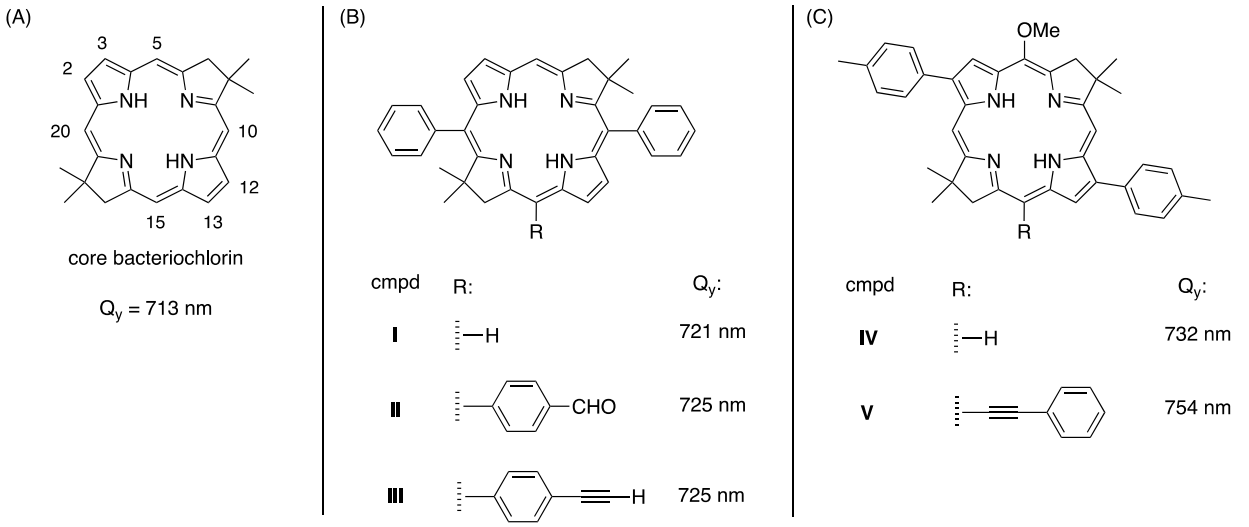

Figure 1. Wavelength tuning in synthetic bacteriochlorins.

B. Composing bacteriochlorin dyads. To limit steric hindrance in the phenylethyne-linked dyads, we chose to locate the y-axis auxochromes at the 2,12- rather than the more explored 3,13-positions, with the assumption that the shift in wavelength would be nearly identical for the two sets of positions. This assumption was based on the results of substituents (bromo,[61] ester,[61] acetyl,[62] branched alkyl[63]) at the 2,12-positions of bacteriochlorins. We also assumed the effects of 2,12-substituents and the meso-substituent (due to the linker) would be additive.

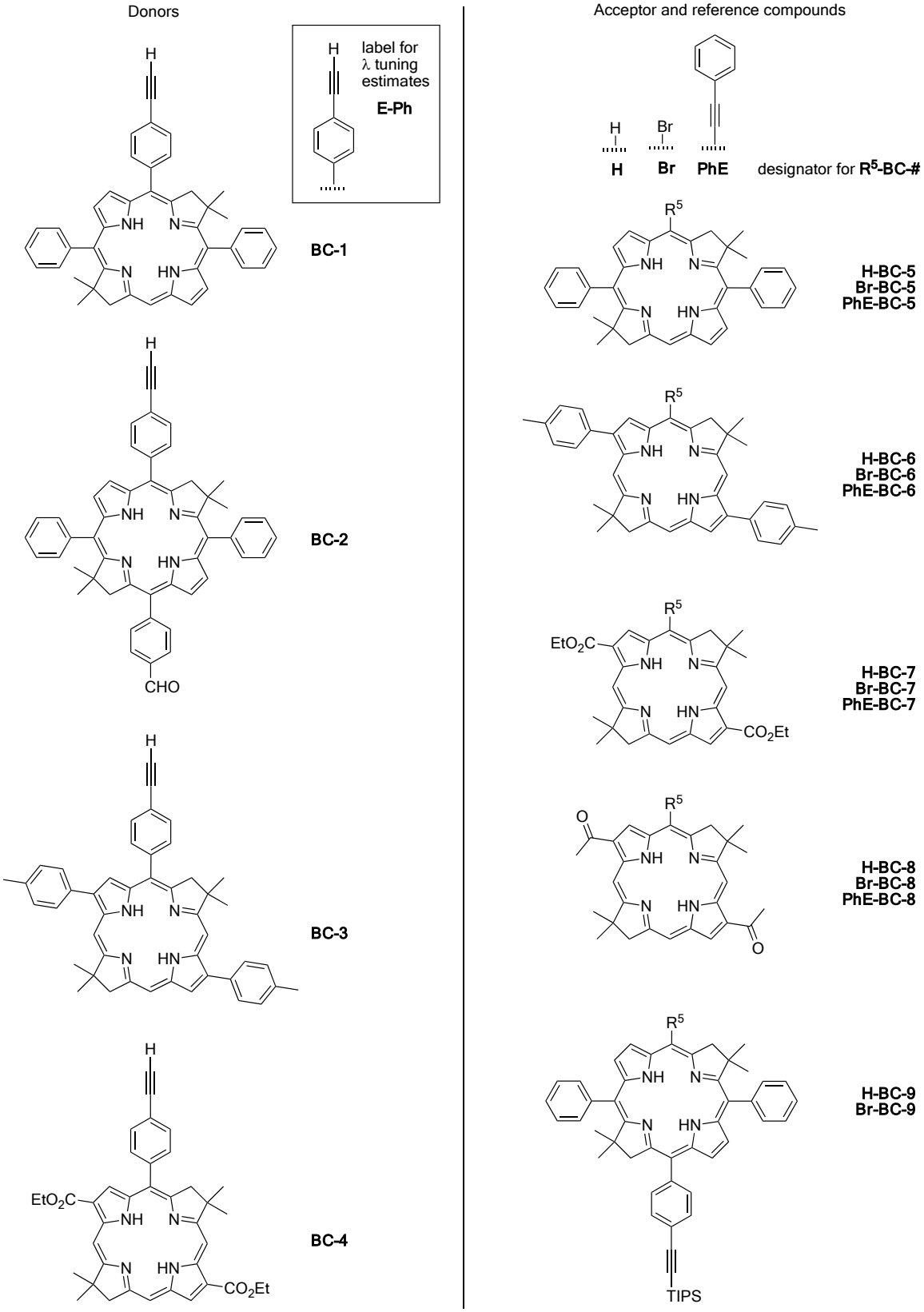

Chart 2. Bacteriochlorin donors (left) and acceptors (right).

The bacteriochlorin donors are shown in Chart 2. The predicted position of the Q_y band is listed in Table 2 along with the observed position. Bacteriochlorin **BC-1** is equipped with 10,20-diphenyl groups (725 nm observed), **BC-2** contains 10,20-diphenyl groups as well as a 15-(4-formylphenyl) group (730 nm observed), **BC-3** contains 2,12-di-*p*-tolyl groups (741 nm observed), and **BC-4** contains 2,12-dicarboethoxy groups (757 nm observed).[62] In each case, the observed position of the Q_y band is within 2 nm of the prediction on the basis of additivity of substituent effects.

Table 2. Donor bacteriochlorin molecular design.

bacteriochlorin	Predicted λ (nm)	Observed λ (nm)
BC-1[a]	713 + 8 ($Ph^{10,20}$) + 5 ($E\text{-}Ph^{5}$) = 726	725
BC-2	713 + 8 ($Ph^{10,20}$) + 5 ($E\text{-}Ph^{5}$) + 5 ($OHC\text{-}Ph^{15}$) = 731	730
BC-3	713 + 23 ($H_3C\text{-}Ph^{2,12}$) + 5 ($E\text{-}Ph^{5}$) = 741	741
BC-4	713 + 41 ($EtO_2C^{2,12}$) + 5 ($E\text{-}Ph^{5}$) = 759	757

[a]**BC-1** and **III** are the same compound.

The acceptors were designed on the basis of known substituent effects including the expected 22 nm bathochromic shift imparted by the ethyne-attached phenylethynyl group. The bacteriochlorin acceptors were designed to complement the bacteriochlorin donors so that ultimately a set of dyads could be prepared wherein the donor–acceptor energy gap ranged from nearly zero to as large as possible within the constraints of minimally substituted chromophores. The acceptor reference compounds that contain the desired auxochromes as well as the phenylethynyl substituent (to mimic the role of the linker in dyads) are shown in the right panel of Chart 2. The chart includes bacteriochlorin scaffolds (**H-BC-5**,[64] **H-BC-6**,[65] **H-BC-7**,[61] **H-BC-8**,[62] and **H-BC-9**[62]), 5-bromobacteriochlorin building blocks (**Br-BC-5**,[64] **Br-BC-6**,[62] **Br-BC-7**,[62] **Br-BC-8**,[62] and **Br-BC-9**[62]), and 5-(phenylethynyl)bacteriochlorin reference compounds. The

latter four reference bacteriochlorins (**PhE-BC-5 – PhE-BC-8**) were synthesized to validate the predictions on the basis of the effects of substituent additivity on wavelength position and for spectroscopic studies, and are reported herein. The predicted Q_y band position ranges from 743–786 nm. The predicted and observed Q_y band positions of the 5-(phenylethynyl)bacteriochlorins are provided in Table 3. In each case, the observed position was within 4 nm of the prediction. (We describe the data of the new reference bacteriochlorins **PhE-BC-5 – PhE-BC-8** in this section to best inform understanding the design of the bacteriochlorin dyads.) Bacteriochlorin building block **Br-BC-9** was used without a corresponding phenylethyne-substituted reference (**PhE-BC-9**). The Q_y band of **PhE-BC-9** was predicted to appear at 748 nm on the basis of **PhE-BC-5** along with a 5-nm bathochromic shift imparted by the 4-(TIPS-ethynyl)phenyl substituent at the bacteriochlorin meso-position. The absorption spectra of bacteriochlorins **BC-1 – BC-4** and **PhE-BC-5 – PhE-BC-8** are shown in Figure 2. In summary, the donors and acceptors exhibit the Q_y band ranging from 725–757 nm and 743–786 nm, respectively.

Table 3. Acceptor bacteriochlorin molecular design.

Phenylethynyl-BC	**Predicted λ (nm)**	**Observed λ (nm)**
PhE-BC-5 (**I** or **H-BC-5**)[a]	713 + 8 ($Ph^{10,20}$) + 22 (PhE^5) = 743	743 (721)
PhE-BC-6 (**H-BC-6**)[a]	713 + 23 (H_3C-$Ph^{2,12}$) + 22 (PhE^5) = 758	756 (737)[58]
PhE-BC-7 (**H-BC-7**)[a]	713 + 41 ($EtO_2C^{2,12}$) + 22 (PhE^5) = 776	774 (755)[54]
PhE-BC-8 (**H-BC-8**)[a]	713 + 55 ($Ac^{2,12}$) + 22 (PhE^5) = 790	786 (768)[55]

[a]The bacteriochlorin lacking a phenylethynyl group.

The rationale for use of both a 4-formylphenyl group and a 4-(TIPS-ethynyl)phenyl group stems from a synthetic subtlety, as both impart a bathochromic shift of ~5 nm. The 4-formylphenyl group was introduced as the fourth aryl substituent to form *donor* bacteriochlorin **BC-2**; a polar substituent was essential to facilitate separation of the monomeric bacteriochlorin from unwanted byproducts. Thus the 4-formylphenyl group provides two functions: enhanced purification and tuning of the wavelength. The 4-(TIPS-ethynyl)phenyl group was employed with *acceptor* bacteriochlorin **Br-BC-9**, which was conveniently obtained from the precursor to **BC-1**. The presence of the TIPS group was essential to mask the ethyne during the Suzuki reaction and then be removed to conduct the subsequent Sonogashira coupling reaction. In principle, the 4-formylphenyl group could have been employed in both instances, but would have required additional synthesis as **BC-1** and **BC-2** were both derived from 4-(TIPS-ethynyl)phenyl-linked **Br-BC-9**.[62] For consistency, the linker or site of linker attachment is designated as the 5-position, and the meso-positions flanking the gem-dimethyl groups occupy the 10- and 20-positions.

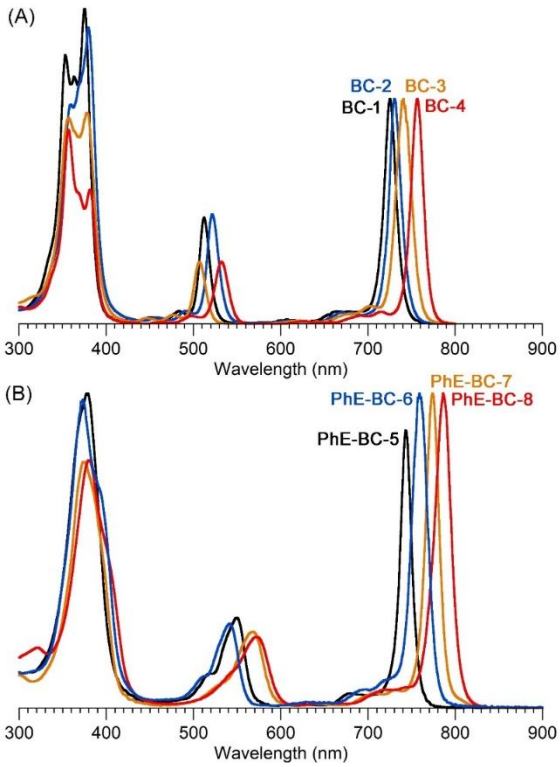

Figure 2. Absorption spectra of reference acceptors and donors.

2. Synthesis of bacteriochlorin benchmarks and dyads

The syntheses of the phenylethyne-linked bacteriochlorin acceptor reference compounds and the bacteriochlorin dyads entailed a Sonogashira reaction[66] of a 5-bromobacteriochlorin and the 5-(4-ethynylphenyl)bacteriochlorin. The bromobacteriochlorin building blocks **Br-BC-5**,[64] **Br-BC-6**,[62] **Br-BC-7**,[62] and **Br-BC-8**[62] were synthesized previously. The synthesis of the phenylethyne-linked bacteriochlorin acceptor reference compounds is shown in Scheme 1. The Sonogashira reaction was carried out under conditions that support dilute reactants (here, ~1 mM of each bacteriochlorin was employed) in the absence of any copper cocatalyst[67] so as to avoid adventitious copper metalation of the free base bacteriochlorins (unlike copper, palladium does not afford facile metalation of tetrapyrrole macrocycles). Such conditions resemble those for constructing phenylethyne-linked porphyrins and phthalocyanines.[68,69] The reaction of 5-bromobacteriochlorins with a phenylethyne group has been examined previously.[60]

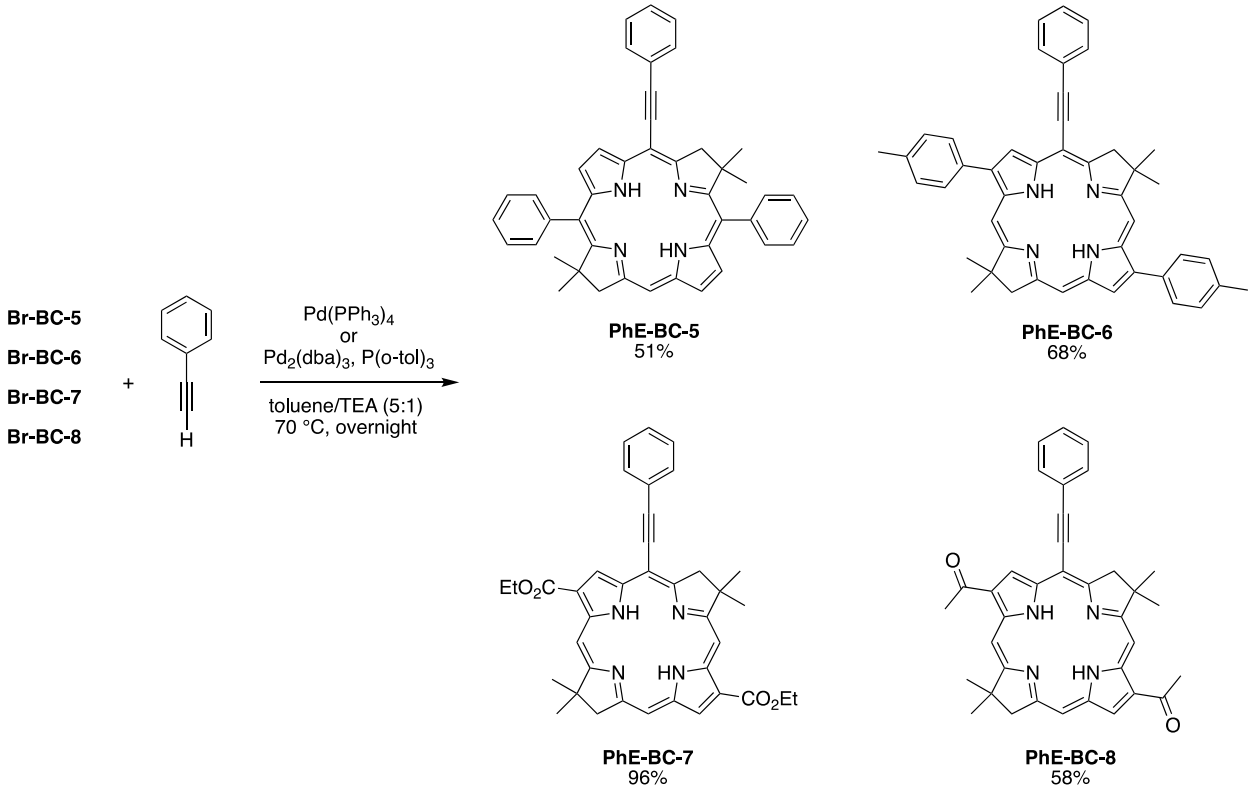

Scheme 1. Synthesis of phenylethynyl-linked bacteriochlorin reference compounds.

The synthesis of the bacteriochlorin dyads is shown in Scheme 2. The combination of bacteriochlorin building blocks for each of the nine dyads is listed in Table 4. For the syntheses of **Dyad-1** and **Dyad-4**, the crude reaction mixture following the Sonogashira coupling was treated with TBAF to remove the TIPS protecting group and reveal the 4-ethynylphenyl group. The 4-ethynylphenyl group serves as an auxochrome (bathochromic shift of ~5 nm), and the terminal methine proton conveniently resonates at δ 3.5 ppm in the ^{1}H NMR spectrum, which provides a useful signal during chemical characterization. The 4-formylphenyl group also gives a distinct signature at ~10 ppm in the ^{1}H NMR spectrum.

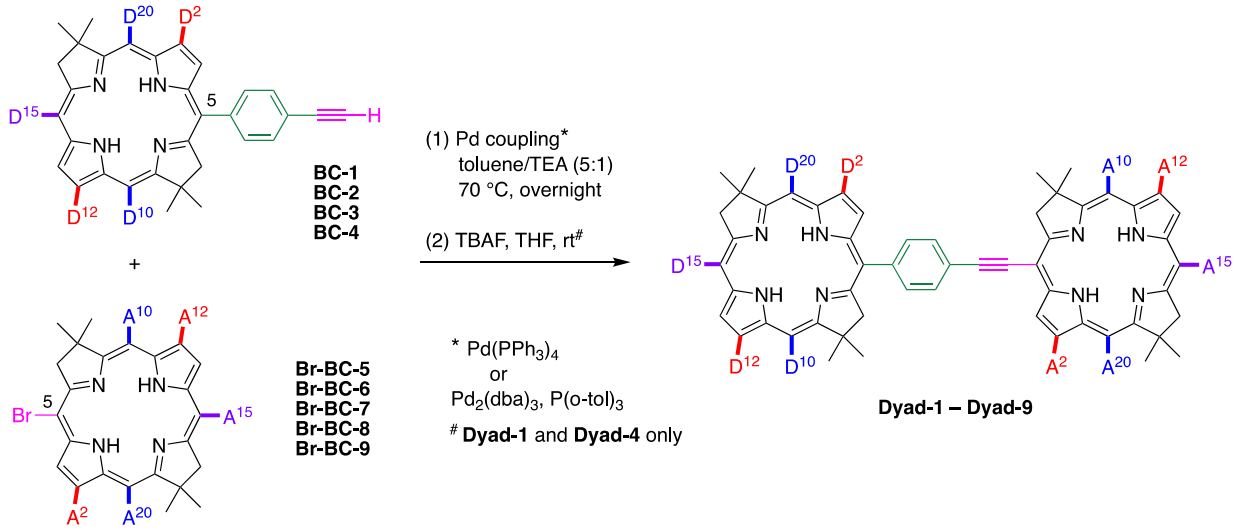

Scheme 2. Synthesis of phenylethynyl-linked bacteriochlorin dyads.

Table 4. Spectral data for bacteriochlorin building blocks and dyads.[a]

Dyad	Donor	Acceptor	Mon[b] λ_D (nm)	Mon[c] λ_A (nm)	Predicted[d] $\lambda_A - \lambda_D$ (nm) [cm^{-1}]	Dyad[e] λ_D (nm)	Dyad[f] λ_A (nm)	Observed[g] $\lambda_A - \lambda_D$ (nm) [cm^{-1}]	Calculated[h] $\lambda_A - \lambda_D$ (nm) [cm^{-1}]
1	**BC-3**	**Br-BC-9**	741	748	7 [126]	741	752	11 [197][i]	14 [238]
2	**BC-2**	**Br-BC-5**	730	743	13 [240]	731.6	744.4	13 [235]	15 [277]
3	**BC-4**	**Br-BC-7**	757	776	19 [323]	757.0	774.8	18 [303]	24 [394]
4	**BC-2**	**Br-BC-9**	725	743	18 [334]	731.6	750.0	18 [335]	22 [394]
5	**BC-1**	**Br-BC-5**	730	748	18 [330]	725.2	743.8	19 [345]	22 [408]
6	**BC-1**	**Br-BC-6**	725	758	33 [600]	725.2	759.8	35 [628]	39 [699]
7	**BC-2**	**Br-BC-7**	730	776	46 [812]	730.8	774.5	44 [772]	50 [863]
8	**BC-1**	**Br-BC-7**	725	776	51 [907]	725.4	774.6	49 [876]	58 [1006]
9	**BC-1**	**Br-BC-8**	725	790	65 [1135]	725.2	787.4	62 [1089]	67 [1153]

[a]All spectral data are for compounds in toluene at room temperature. [b]Q_y maximum of building block donor monomer (column 2). [c]Q_y maximum of acceptor building block monomer (column 3) but with the bromine atom replaced with a phenylethynyl group (Chart 2). [d]Donor–acceptor Q_y wavelength [wavenumber] gap from monomers. [e]Q_y maximum of donor in the dyad. [f]Q_y maximum of acceptor in the dyad. [g]Measured donor–acceptor Q_y wavelength [wavenumber] gap in the dyad. [h]Donor–acceptor Q_y wavelength [wavenumber] gap for dyad obtained from TDDFT calculations. [i]From a two-Gaussian fit.

The energy gap of the nine dyads ranges from ~200 to ~1100 cm^{-1}. Brief comments concerning the design of the dyads are presented next, in order of small to large energy gap.

- To create a very small energy gap with phenylethyne-linked bacteriochlorins requires, counterintuitively, a parent donor (**BC-3**, 741 nm) with a longer wavelength Q_y band versus that of the parent acceptor (**BC-9**, 725 nm),[62] given that the Q_y band of the acceptor is bathochromically shifted (to ~750 nm) upon attachment to the ethynyl unit of the linker. Thus, joining donor **BC-3** (2,12-di-*p*-tolyl groups) with acceptor **Br-BC-9** (10,20-diphenyl-15-(4-TIPS-ethynyl) groups) afforded **Dyad-1**, with $\Delta Q_y \sim 200$ cm^{-1}.
- The next smallest energy gap was obtained by use of **BC-2** and **Br-BC-5** to form **Dyad-2** ($\Delta Q_y \sim 235$ cm^{-1}), wherein both bacteriochlorins bear 10,20-diphenyl groups but the donor alone is equipped with a 15-(4-formylphenyl) unit.

- A slightly larger energy gap was achieved upon use of identical bacteriochlorins for the donor and acceptor constituents. Thus, 2,12-dicarboethoxy substituents in both donor and acceptor (**BC-4**, **Br-BC-7**) afforded **Dyad-3**, with $\Delta Q_y = 303$ cm^{-1}.
- The next dyad in the series relied on triaryl substitution for each bacteriochlorin. The donor bacteriochlorin (**BC-2**) has 10,20-diphenyl-15-(4-formylphenyl) groups, whereas the acceptor bacteriochlorin (**Br-BC-9**) has 10,20-diphenyl-15-(4-(TIPSethynyl)phenyl) groups, which yielded **Dyad-4** with $\Delta Q_y = 335$ cm^{-1}.
- A slightly larger energy gap was again achieved upon use of identical bacteriochlorins for the donor (**BC-1**) and acceptor (**Br-BC-5**) constituents. The use of 10,20-diphenyl substituents in both donor and acceptor afforded **Dyad-5** with $\Delta Q_y = 345$ cm^{-1}. As in the case of **Dyad-3**, the difference in position of the respective Q_y bands stems entirely from the unsymmetric auxochromic effects of the phenylethyne linker.
- An energy gap larger than that imparted solely by the unsymmetric auxochromic effect of the phenylethyne linker is more readily obtained by use of a parent donor that absorbs at shorter wavelength than the parent acceptor. Thus, the combination of 10,20-diphenylbacteriochlorin (**BC-1**) and 2,12-di-*p*-tolylbacteriochlorin (**Br-BC-6**) afforded **Dyad-6** with $\Delta Q_y = 628$ cm^{-1}. Similarly, combination of the 10,20-diphenyl-15-(4-formylphenyl)bacteriochlorin (**BC-2**) and 2,12-dicarboethoxybacteriochlorin (**Br-BC-7**) afforded **Dyad-7**, with $\Delta Q_y = 772$ cm^{-1}.
- The last two dyads relied on a common donor (10,20-diphenylbacteriochlorin, **BC-1**) and the 2,12-dicarboethoxybacteriochlorin (**Br-BC-7**) or 2,12-diacetylbacteriochlorin (**Br-BC-8**) to afford **Dyad-8** or **Dyad-9** with $\Delta Q_y = 876$ cm^{-1} or 1089 cm^{-1}, respectively.

In summary, the use of four donors and five acceptors enabled construction of a set of dyads with progressively tuned donor–acceptor ΔQ_y bands across the ~200–1100 cm^{-1} range. Donor bacteriochlorins **BC-1** and **BC-2** together were employed seven times, with

bacteriochlorins **BC-3** and **BC-4** each employed once. On the acceptor side, **Br-BC-7** was used three times, **Br-BC-9** and **Br-BC-5** were each used twice, and **Br-BC-6** and **Br-BC-8** were each used once. Together, the nine building blocks were used to create 9 of the possible 20 dyads.

3. Chemical characterization

The bacteriochlorin dyads and reference acceptors were characterized by ^{1}H NMR and ^{13}C NMR spectroscopy. Quality ^{1}H NMR spectrum were not obtained for **Dyad-1** and **Dyad-4** due to poor solubility. Quality ^{13}C NMR spectra of dyads were only obtained for **Dyad-3** and **Dyad-8**. The presence of the phenylethyne group at the *meso*-position of a bacteriochlorin gives rise to distinct 7- and 17-methylene positions. The difference is greater for the bacteriochlorins proximal to the phenyl versus ethynyl unit of the phenylethyne linker (~0.50 ppm vs ~0.25 ppm). In each dyad, two sets of peaks due to the 7- and 17-methylene groups from the different bacteriochlorin units are found, but the chemical shift differences (~0.4 ppm) are nearly the same for each macrocycle. Each dyad and reference compound was analyzed by electrospray ionization mass spectrometry (ESI-MS), whereupon a singly charged, doubly charged, or protonated molecular ion was observed. Further characterization entailed optical spectroscopy, as described in the next section.

4. Photophysical characterization

A. Static absorption and fluorescence features. The absorption and fluorescence spectra of the benchmark donors and acceptors are collected in Figure 3A. These data are reorganized in Figure 3C to show the overlap between the emission spectrum of the benchmark donor and the absorption spectrum of the benchmark acceptor for each of the nine dyads. The value of the spectral overlap integral (J)[28] obtained as part of the Förster energy-transfer calculations (*vide infra*) is given on Figure 3C. The absorption and fluorescence spectra for all nine dyads are presented in

Figure 3B. The emission spectra were obtained by exciting the donor constituent in its Q_x absorption band (510–535 nm). Figure 3D focuses on the NIR region that contains the Q_y absorption bands of the donor and acceptor constituents. The Q_y feature for the acceptor defines the $S_0 \rightarrow S_1$ transition for the dyad. The Q_y feature for the donor corresponds to the $S_0 \rightarrow S_2$ transition for the dyad. The Q_y absorption bands of the donor and acceptor are substantially overlapped for **Dyad-1**. Consequently, peak positions were derived from fitting the NIR absorption profile to the sum of two Gaussians. The resultant $S_2 - S_1$ excited-state energy gap is given on Figure 3D. The value ranges from ~200 cm^{-1} for **Dyad-1** to ~1100 cm^{-1} for **Dyad-9**.

Several observations from Figure 3 are noteworthy. The absorption spectrum of each dyad is basically the superposition of the spectra of the benchmark monomers. This was anticipated from our prior studies of dyads in which two tetrapyrrole macrocycles are joined by a phenylethyne linker.[68-70] Upon excitation of the donor, fluorescence from the dyad occurs primarily from the acceptor. This indicates rapid and efficient energy transfer from the donor to the acceptor. A small amount of the total emission appears to derive from the donor for **Dyad-1** (Figure 3D). This likely reflects thermal equilibrium between the lowest singlet excited states of the donor and acceptor given that the energy gap is comparable to thermal energy (~210 cm^{-1}). Some donor emission may also occur for **Dyad-2** – **Dyad-5**, but to a decreasing extent as the energy gap gets progressively larger than kT.

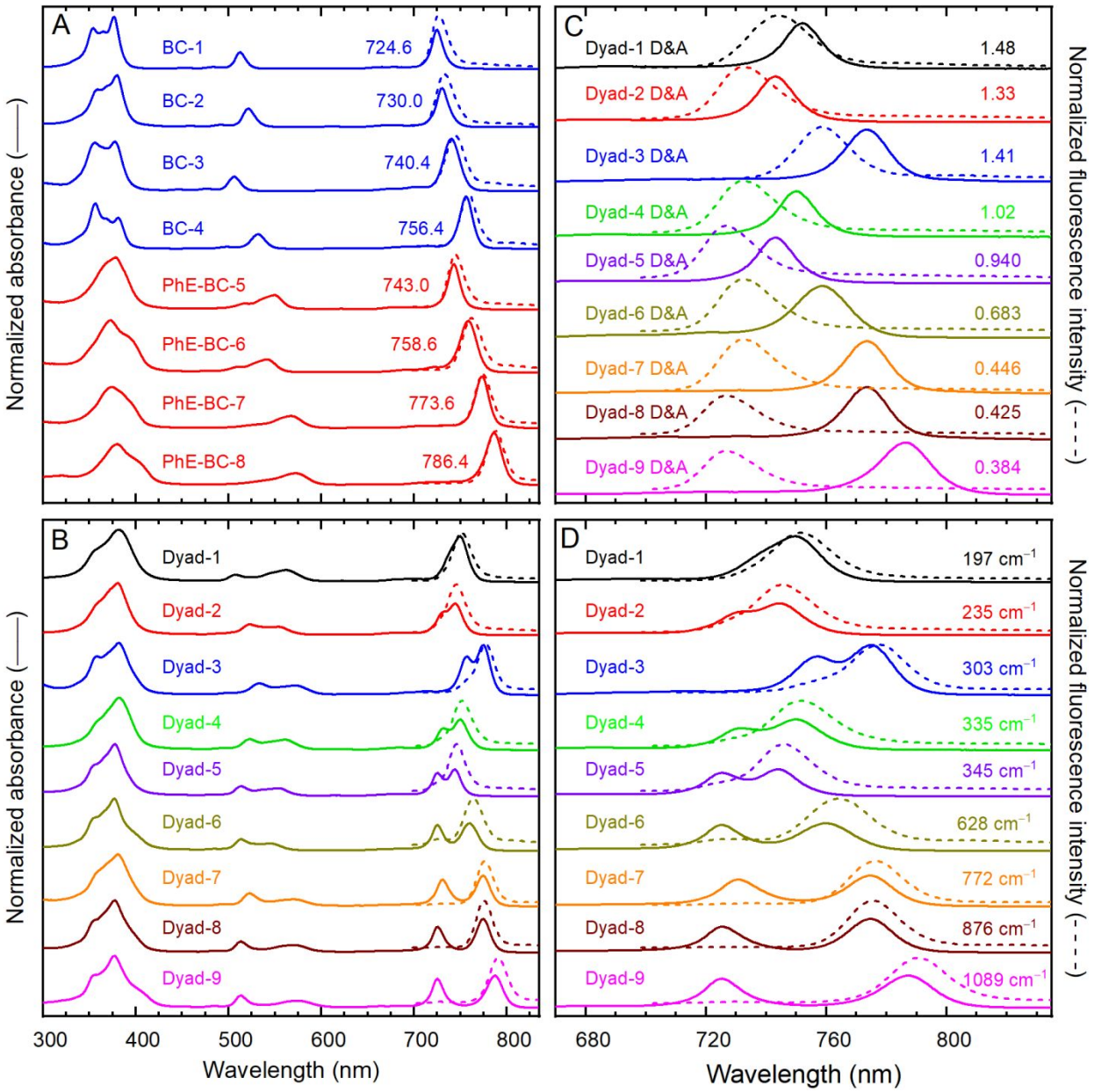

Figure 3. Absorption (solid) and fluorescence spectra (dashed) of the benchmark donors and acceptors (A and C) and dyads (B and D) in toluene at room temperature. Panel C shows the overlap of the emission spectrum of the benchmark donor and absorption spectrum of the benchmark acceptor along with the value of the spectral overlap integral (J x 10^{-12} cm^6 $mmol^{-1}$) used in the Förster calculations. Panel D focuses on the NIR region from panel B and gives the donor–acceptor excited-state energy gap obtained from the corresponding Q_y maxima. To obtain fluorescence emission spectra, dyads were excited at the Q_x band (~500–600 nm) of the donor, while monomers were excited at their Q_x band (~500–600 nm). Emission spectra were also recorded after excitation at the Soret region (~350–400 nm, not shown) and had similar spectral features as those obtained after Q_x excitation.

B. Fluorescence yield and S_1 lifetime. The fluorescence yields of benchmark donors and acceptors in toluene range from 0.14 to 0.22 (Table 5). The Φ_f values for the dyads are similar and correspond to fluorescence from the acceptor constituent. The Φ_f for each dyad is the same within experimental error whether the donor, the acceptor, or both was excited, reflecting efficient energy transfer from donor to acceptor bacteriochlorin.

Table 5. Excited-state properties.[a]

Compound	λ_{em} (nm)[b]	Φ_f	τ_S (ns)
Donor Monomers			
BC-1	727	0.19	3.8
BC-2	732	0.21	4.3
BC-3	745	0.22	3.1
BC-4	758	0.19	3.4
Acceptor Monomers			
PE-BC-5	745	0.22	4.3
PE-BC-6	762	0.22	3.7
PE-BC-7	774	0.19	3.6
PE-BC-8	788	0.14	2.9
Dyads			
1	751	0.25	4.0
2	745	0.22	4.0
3	777	0.20	3.2
4	751	0.24	4.1
5	746	0.21	4.1
6	764	0.23	3.5
7	777	0.20	3.6
8	776	0.19	3.5
9	790	0.16	2.8

[a]All measurements were in Ar-purged toluene at room temperature. [b]The fluorescence emission maximum for the dyads is for the energy acceptor because emission from the donor is quenched by energy transfer to the acceptor.

Table 5 also lists the singlet excited-state lifetimes for the benchmark donors and acceptors in toluene. These values were determined by time correlated single photon counting (TCSPC) and range from 2.9 to 4.3 ns. Representative decay profiles and fits are given in Figure S10. The τ_S value for each dyad is the S_1 lifetime of the excited acceptor, formed by direct excitation or energy

transfer from the donor. The lifetime of the excited acceptor in a given dyad determined by TCSPC is in good agreement with that obtained by transient absorption (TA) spectroscopy. TA spectrocopy was also used to obtain the lifetime of the excited donor in each dyad, which afforded the rate constant for excited-state energy transfer (*vide infra*). The Φ_f and τ_S values for each dyad are comparable to the values for the corresponding benchmark acceptor, consistent with the absence of any noticeable quenching of the excited acceptor bacteriochlorin by charge transfer involving the donor.

C. Excited-state energy transfer. Energy transfer from the excited donor to the acceptor for the nine dyads was studied recently.[47] The rate constant for this process (k_{trans}) ranges from ~$(0.3\ ps)^{-1}$ to ~$(1.7\ ps)^{-1}$. The last three columns of Table 6 give the measured k_{trans}, $\tau_{trans} = 1/k_{trans}$, and the donor–acceptor excited-state energy gap derived from the ground-state absorption spectra described above.

Table 6. Parameters for Förster energy-transfer calculations and experimental values.

Dyad	Input Parameters[a]						Output Parameters[b]				Experiment[c]		
#	κ^2	R (Å)	$\Phi_{f(D)}$	τ_D (ns)	ε_A (M^{-1} cm^{-1})	λ_A (nm)	J x 10^{-12} (cm^6 $mmol^{-1}$)	Φ_{trans}	k_{trans} x 10^{11} (s^{-1})	τ_{trans} (ps)	k_{trans} x 10^{11} (s^{-1})	τ_{trans} (ps)	ΔE_{DA} (cm^{-1})
1	0.55	15.3	0.22	3.1	117,479	752	1.48	0.9996	7.82	1.28	3.45	0.29	197
2	0.93	15.1	0.21	4.3	117,479	744.4	1.33	0.9997	8.87	1.13	2.63	0.38	235
3	1.29	15.4	0.19	3.4	135,037	774.8	1.41	0.9998	13.3	0.75	2.44	0.41	303
4	1.06	15.2	0.21	4.3	117,479	750	1.02	0.9997	7.41	1.35	1.75	0.57	335
5	0.94	15.1	0.19	3.8	117,479	743.8	0.940	0.9996	6.47	1.55	1.35	0.74	345
6	0.99	15.2	0.19	3.8	125,596	759.8	0.683	0.9994	4.76	2.10	0.60	1.67	628
7	1.53	15.3	0.21	4.3	135,037	774.5	0.446	0.9995	4.51	2.22	0.93	1.07	772
8	1.35	15.2	0.19	3.8	135,037	774.6	0.425	0.9993	4.04	2.48	0.93	1.07	876
9	1.48	15.2	0.19	3.8	118,361	787.4	0.384	0.9993	3.99	2.50	0.92	1.09	1089

[a]The refractive index of toluene (n = 1.5), the solvent for energy-transfer studies of the dyads, was used for all calculations. [b]The calculations were performed using PhotochemCAD.[71] [c]The experimental τ_{trans} was determined by TA studies of the dyads in Ar-purged toluene at room temperature. The time constant is an amplitude weighted average derived from dual-exponential fits to decay of the donor Q_y bleach decay. This behavior is thought to arise from populations of

the excited donor that are unrelaxed (vibrational, conformational, solvent) and relaxed on the time scale of energy transfer.[47]

D. Förster calculations. The prior study of these dyads probed the impact of vibrational-electronic coherences on the rate of excited-state energy transfer.[47] One part of the study was to elucidate if the measured rate would deviate from a trend-line for dyads wherein a vibrational-electronic resonance was likely. No such correlations were found. Any deviations from the trend-line were small, and generally corresponded to rates that were slower rather than faster than predicted given the results from other members of the set. Another aspect was to compare the measured rates with the values predicted by Förster theory, which assumes incoherent energy transfer driven by the coupling of the transition-dipole moments of the donor and acceptor. The description of the Förster calculations and tabulated input/output parameters were provided in the Supplementary Information accompanying the prior communication.[47] Here, we highlight and delve deeper into the calculations that are most relevant to the molecular design of the dyads and the analysis of energy transfer.

The values of the rate constant for energy transfer, k_{trans}, are plotted in Figure 4A. The calculated Förster rates are plotted as a function of donor–acceptor excited-state energy gap in Figure 4B. Comparison of Figures 4A and 4B show that the measured energy-transfer rates agree with values predicted by Förster theory to within a factor of two, as described previously.[47]

The rate constant for Förster energy transfer from a donor (D) to an acceptor (A) is given by Equation 1.[4,10] Here, κ^2 is the orientation factor pertaining to the TDM vectors of the donor and acceptor;[11] $\Phi_{f(D)}$ and τ_D are the fluorescence yield and singlet excited-state lifetime, respectively, of the donor in the absence of the acceptor;[10] R is the center-to-center distance between the two bacteriochlorins; and n is the refractive index of the intervening medium.[72] Here, n is taken to be that of the solvent (toluene), as is customary; regardless, toluene reasonably

resembles much of the structure of the phenylethyne linker. Equation 2 defines the spectral overlap integral (J), which reflects overlap of the donor fluorescence spectrum [$f_D(\nu)$] and the acceptor absorption spectrum given in units of molar absorptivity [$\varepsilon_A(\nu)$], both spectra being plotted in wavenumber (ν) units (cm^{-1}). The quantum yield of energy transfer is defined by Equation 3.

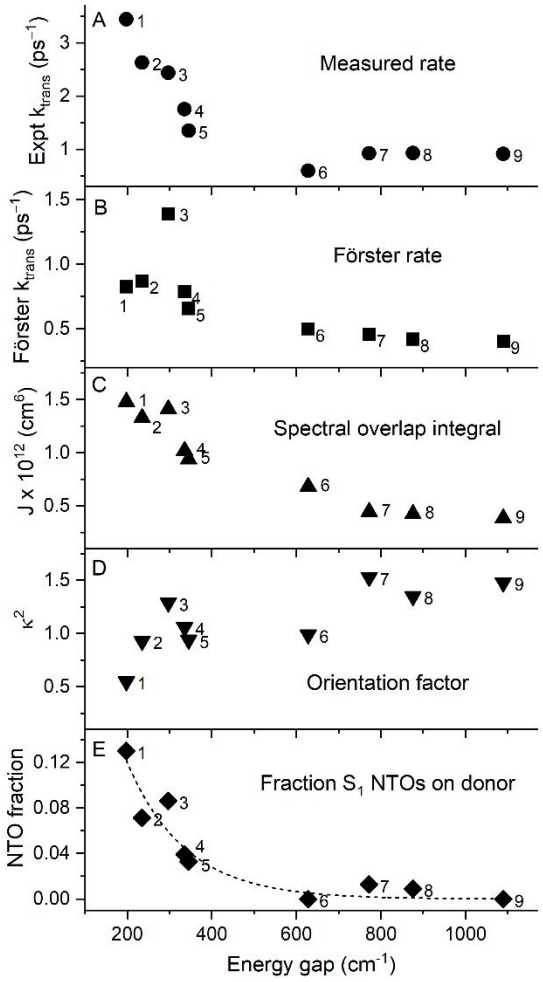

Figure 4. Measured and Förster (calculated) energy-transfer rate constant and parameters versus donor–acceptor excited-state energy gap for nine dyads. The dashed line in panel E is a fit to the function $y = y_0 \exp(-\Delta E / \beta)$ that returns $\beta = 140$ cm^{-1}.

$$k_{trans}(s^{-1}) = 8.8 \times 10^{23} \frac{\kappa^2 \Phi_{f(D)}}{n^4 \tau_D R^6} J \quad (1)$$

$$J = \int_0^{\infty} \frac{f_D(\nu)\varepsilon_A(\nu)}{\nu^4} d\nu \quad (2)$$

$$\Phi_{trans} = \frac{k_{trans}}{\tau_D^{-1} + k_{trans}} \quad (3)$$

The values of the parameters indicated in Equations 1–3 for each dyad are given in Table 6. As noted in the Introduction, the means of obtaining some of the input parameters are not always obvious and misinterpretations are common.[10,28] A generic value often utilized for the relative orientation of the TDM vectors is not applicable when the donor and acceptor are covalently linked. Obtaining a reliable trend in the spectral overlap integrals for a series of molecules such as those studied here depends critically on the method of obtaining the molar absorptivity of the energy acceptor in each case. Thus, an in depth analysis is required. Regardless, the key structure-property relationship for each parameter for the set of dyads is captured and displayed visually in Figure 4. The value of each parameter as well as the resulting calculated and measured energy-transfer rate for each dyad are plotted versus the donor–acceptor energy gap. The energy gap for each dyad in turn is dictated by the choice of substituents on the bacteriochlorin donor and acceptor constituents (Chart 1). These considerations are explored in the following subsections.

i. Spectral overlap term. The input spectra used to obtain the spectral overlap integral (J) are plotted in Figure 3C. It is noteworthy here that obtaining the J value requires knowledge of the molar absorptivity of the acceptor at some wavelength (ε_A).[28] These values typically carry large uncertainty, which can impart uncertainty to the assessment of trends in spectral properties.[73] The method utilized to obtain the Q_y extinction coefficient for each bacteriochlorin monomer is as follows.[47,73] The integrated Q_y absorption manifold and the Q_y oscillator strength (f) obtained from TDDFT calculations for a given monomer were compared with those values for 5-methoxy-8,8,18,18-tetramethyl-2,12-di-*p*-tolylbacteriochlorin, which has measured[65] Q_y peak ε = 120,000 $M^{-1}cm^{-1}$. This method provides an internally consistent set of ε values for the set of dyads. The relevant values are listed in Figure 5, which shows the spectra for the donor and acceptor bacteriochlorins plotted with the intensity being molar absorptivity.

Figure 3C shows how the use of substituents on the donor and acceptor bacteriochlorins progressively reduces the overlap of the donor $S_1 \rightarrow S_0$ fluorescence and the acceptor $S_0 \rightarrow S_1$ absorption. The resulting value for the spectral overlap value J for each dyad is listed in Table 6 and plotted versus the donor–acceptor excited-state energy gap in Figure 4C. Comparison with Figure 4A shows that the J value and measured k_{trans} value vary by about three-fold between **Dyad-1** and **Dyad-9** and follow the same general trend. This is expected because the rate is linear with J within Förster theory (Equation 1).

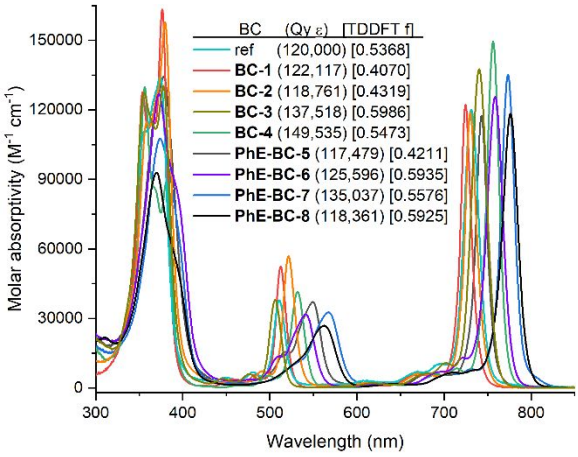

Figure 5. Molar absorptivity spectra for benchmark donors and acceptors (Chart 2) and reference compound 5-methoxy-8,8,18,18-tetramethyl-2,12-di-*p*-tolylbacteriochlorin.[65]

ii. Orientation factor. A key parameter in the Förster calculations is the orientation factor κ^2. Often this value is not known for a FRET pair and the isotropic dynamically averaged value of 2/3 is utilized. The term "dynamically averaged" refers to the case where each donor–acceptor pair (typically with no covalent donor–acceptor linker) explores all 3-dimensional conformations during the lifetime of the donor excited state.[74] While perhaps rarely obtained in many FRET experiments, the 2/3 value is widely used.[11]

Here, the κ^2 value for each dyad was obtained by first calculating the minimum energy structure by DFT of the dyad, and then identifying the location of the transition-dipole moment in

each of the two bacteriochlorins via TDDFT calculations. The minimum-energy structure for **Dyad-5** obtained from the DFT calculations is shown in Figure 6. The two bacteriochlorins joined via the phenylethyne linker are essentially (but not precisely) perpendicular to one another. The value of κ for each dyad was obtained using Equation 4 and the angles for the TDM vectors of the donor and acceptor with respect to each other (θ_{AD}) and the centerline (θ_A and θ_D), as defined in Figure 7 and outlined previously.[47] The values of θ_A and θ_D were obtained from TDDFT calculations. Use of the dot-product formula (Equation 5) and the coordinates of the TDM vectors (Table 7) affords the value of θ_{AD}. The values of θ_{AD} are given in Table 8.

$$\kappa = \cos(\theta_{AD}) - 3*\cos(\theta_A)*\cos(\theta_D) \quad (4)$$

$$x_D x_A + y_D y_A + z_D z_A = (x_D^2 + y_D^2 + z_D^2) \times (x_A^2 + y_A^2 + z_A^2) \times \cos(\theta_{AD}) \quad (5)$$

$$\kappa = \sin(\theta_A)\sin(\theta_D)\cos(\phi) - 2\cos(\theta_A)\cos(\theta_D) \quad \text{[if TDM vectors are in plane]} \quad (6)$$

$$\langle\kappa^2\rangle = \tfrac{1}{2}\sin^2\theta_A \sin^2\theta_D + 4\cos^2\theta_A \cos^2\theta_D \quad \text{(restricted dynamic average)}[74] \quad (7)$$

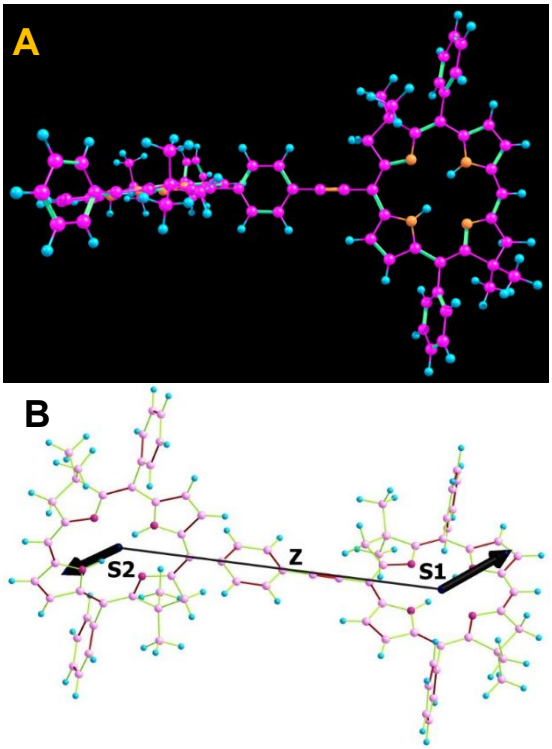

Figure 6. (A) Calculated minimum energy structure of **Dyad-5** wherein the donor bacteriochlorin macrocycle (left) is essentially perpendicular to that for the acceptor (right). (B) TDM vectors for the S_1 (acceptor) and S_2 (donor) excited states of **Dyad-5**; the center-to-center axis is labeled Z.

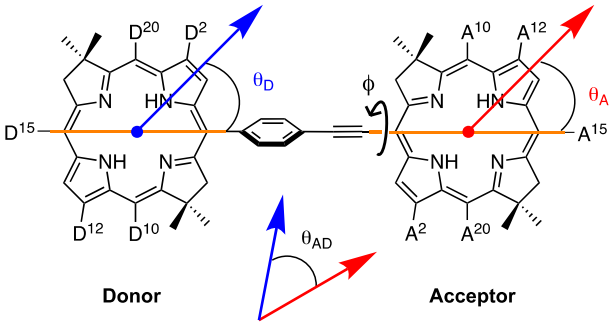

Figure 7. Generic bacteriochlorin donor-acceptor dyad showing the angles required to calculate the orientation factor (κ^2) in Förster energy-transfer theory. The angles for **Dyad-1** – **Dyad-9** are given in Table 8.

Table 7. Coordinates for transition-dipole vectors of donor (D) and acceptor (A) in each dyad.

Dyad	x_D	y_D	z_D	x_A	y_A	z_A
1	–3.4628	–0.3164	–2.1913	1.7652	–2.8191	0.3551
2	1.8385	1.0139	–1.7172	3.0631	2.3797	0.6419
3	2.0412	2.4697	0.8789	–3.9194	1.2983	–1.6978
4	–2.0934	–1.2271	–1.5842	–3.2025	–2.1522	0.8886
5	–1.9595	–1.3009	1.6717	2.7554	2.2062	1.0610
6	–2.1923	–0.5904	–2.1302	2.8043	2.8850	–0.6421
7	–2.2501	–2.2679	–0.4189	–3.3600	0.9792	–2.1875
8	–2.1125	–2.1696	–0.8127	-3.3487	–0.3902	2.2847
9	–2.1839	–2.3274	0.0461	–3.2400	0.6181	–2.3489

Table 8. Angles for transition-dipole-moment vectors and derived orientation factors for dyads.

A	B	C	D	E	F	G	H	I
Dyad	θ_D (deg)	θ_A (deg)	θ_{AD} (deg)	κ	κ^2 (actual)[a]	κ^2 (ϕ = 0° & TDMs in plane)[b]	κ^2 (ϕ = 90° & TDMs in plane)[c]	$\langle\kappa^2\rangle$ (restricted dynamic average)[d]
1	118.182	33.616	115.869	0.7435	0.55	1.62	0.62	0.74
2	46.178	38.986	49.384	–0.9637	0.93	0.39	1.16	1.26
3	52.886	149.523	114.076	1.1363	1.29	2.09	1.08	1.16
4	44.188	36.796	46.231	–1.0308	1.06	0.53	1.32	1.41
5	133.624	40.224	127.643	0.9696	0.94	2.31	1.11	1.22
6	44.697	135.016	120.739	0.9972	0.99	2.26	1.01	1.13
7	45.134	36.256	61.937	–1.2362	1.53	0.52	1.29	1.38
8	133.415	142.608	61.647	–1.1632	1.35	0.42	1.19	1.29
9	46.025	37.885	64.674	–1.2163	1.48	0.43	1.20	1.30

[a]Obtained using Eqs. 4 and 7 and the θ_A, θ_D and θ_{AD} values given in columns B–D. [b]Obtained using Equation 6, θ_A and θ_D values given in columns B–D, and assuming coplanar macrocycles (ϕ = 0°) and TDM vectors in plane. [c]Obtained using Eq. 6, θ_A and θ_D values given in columns B–D, and assuming orthogonal macrocycles (ϕ = 90°) and TDM vectors in plane. [c]Obtained using Equation 7, θ_A and θ_D values given in columns B–D.

The substituents on the donor and acceptor bacteriochlorins in the dyads (as in the corresponding benchmark monomers) rotate the TDM vectors off the traditional y-axis that connects the pair of protonated central nitrogen atoms (the NH–NH axis). The associated deviations of angles θ_A and θ_D (Figure 7) from 45° or 135° are seen in Table 8. The TDM vectors lie out of the macrocycle plane by up to ~15° depending on substituents (e.g., Figure 6B). Additionally, steric interactions involving the macrocycle substituents and the linker result in the donor and acceptor macrocycles deviating from coplanarity by up to ~15°. These factors are all accounted for in the values for κ and κ^2 obtained using the minimum energy structures (e.g., Figure 6), the angles defined in Figure 7, the TDM characteristics listed in Tables 7 and 8, and Equations 4 and 5. The κ^2 values for the dyads are listed in column F of Table 8 (and the second column of

Table 6) and range from 0.55–1.53. An easily visualized display of the out-of-plane component of the TDMs is quite difficult to render with the line drawings of the structures (Figure 7), or even in the calculated ball-and-stick models (Figure 6), but is clearly implied by the non-zero values of z_A shown in the rightmost column of Table 7.

Reference data are useful to put the observed range of κ^2 values in perspective. Here it is useful to consider the alternate formula for κ^2 given in Equation 6 that makes use of the "twist" angle ϕ between donor and acceptor macrocycle planes defined in Figure 7. Equation 6 assumes that the TDM vectors are in the planes of the respective macrocycles. Using that assumption, if the donor and acceptor macrocycle planes were coplanar ($\phi = 0$) and the TDM vectors were aligned along the NH–NH axes, the κ^2 value would be 0.25 or 2.25 depending on the combination 45° and 135° used for θ_A and θ_D. Using the actual values for θ_A and θ_D affords κ^2 values that range from 0.39 to 2.31 (Table 8, column G) with the differences from 0.25 and 2.25 that reflect deviations of TDM vectors from the NH–NH axis. Assuming again that the TDM vectors are in plane, if the macrocycles were orthogonal ($\phi = 90°$) and the TDM vectors were aligned along the NH–NH axes, the value of κ^2 would be 1. For orthogonal macrocycles and allowing the TDM vectors to rotate off the NH–NH axes to assume the values of θ_A and θ_D found for each dyad (Table 8), the value of κ^2 would be in the range 0.62–1.32 (Table 8, column H). The value for each dyad, the κ^2 assuming $\phi = 90°$ deviates from the actual value (0.53–1.53) by about 20%, which reflects the fact that the macrocycles are not perfectly orthogonal and the TDM vectors are not precisely in the plane of each macrocycle.

It is also useful to consider the restrictions on the range of κ^2 values imposed by the presence of the linker joining the donor and acceptor. Not all possible values of ϕ, θ_A and θ_D are permissible to obtain the isotropic dynamically averaged $\kappa^2 = 2/3$ often employed in Förster calculations assuming unrestricted motion. Equation 7 gives what can be considered a restricted

dynamically average value of κ^2 if rotation of the donor and acceptor TDM vectors generate two cones about the linker axis. This is Model 4, Case 1 and Equation 31 of the report by Dale and Eisinger.[74] Any combination of values of 45° and 135° for θ_A and θ_D in Equation 7 gives κ^2 =1.125. If one uses the actual values of θ_A and θ_D for the dyads (Table 8), the values of κ^2 are in the range 0.74–1.41 (Table 8, column I).

Summarizing, examination of the last three columns of Table 8, all of which employ the actual values of θ_A and θ_D for the dyads, is revealing. Dynamic averaging constrained by the presence of the linker gives κ^2 in the range 0.74–1.41. Perfectly orthogonal macrocycles and TDM vectors precisely in plane give κ^2 in the range 0.62–1.32. The actual range of κ^2 obtained from the minimum energy structures is 0.55–1.53. These comparisons show that the range of κ^2 values is dominated by the electronic effects of the substituents on the TDM vectors in the donor and acceptor macrocycles, along with restrictions on their mutual orientation due to the presence of the linker.

Regarding the last point above, calculations performed on the same dyads in which the two bacteriochlorins are coplanar show that energy of the conformation is only slightly greater (300 cm^{-1}) than that for the perpendicular orientation. Given that thermal energy is 207 cm^{-1} at 295 K, the dynamics may afford a distribution of orientations of the respective bacteriochlorins in the dyad architecture. However, the results given in the last column of Table 8 suggest that such motions will not result in a spread of κ^2 values among the dyads significantly different than the spread caused by the differences in substituents utilized. It is interesting to note that a 300 cm^{-1} barrier between orthogonal to coplanar macrocycles connected by the phenylethyne linker should roughly correspond to a torsional mode of about 30 cm^{-1}.[75] The associated period of motion of roughly 1 ps is on the same time scale as energy transfer (Table 6 and Figure 4A). In short, any

dynamical averaging would not be complete on the time scale of energy transfer. Thus, such torsional motions may contribute to the observed non-exponential energy transfer dynamics.[47]

The values of the orientation factor κ^2 are plotted versus the donor–acceptor excited-state energy gap in Figure 4D. Comparison with Figure 4C shows that the trends in the value of κ^2 are generally opposite those in the value of the spectral-overlap integral J. This effect moderates the overall trend in the calculated k_{trans} values (Figure 4B) given that the rate is linear in both J and κ^2 (Equation 1). One can immediately see from this comparison and the analysis given above the error in the predicted energy-transfer rate (k_{trans}) and efficiency (Φ_{trans}) that would have resulted by simply using the same (e.g., averaged) orientation factor for all nine dyads.

iii. Distance of separation. A final note concerns the values input into the Förster calculations for the donor–acceptor distance R. The center-to-center distance R between donor and acceptor bacteriochlorins obtained from the energy-minimized structures (from DFT calculations) for each dyad was utilized (Table 6), following common practice in the point-dipole approximation. However, given the relatively short distance and the size of the macrocycles, this conventional choice may not be applicable if the point-dipole approximation that underlies Equation 1 breaks down.[76] In this regard, it was noted above that the calculated Förster k_{trans} values are on the average about two-fold smaller than the experimental k_{trans} values (Table 6). As described previously,[47] given the $1/R^6$ dependence of the rate on distance (Equation 1), replacing the center-to-center distances (15.3 Å average) by values 11% smaller (13.6 Å average) decreases the predicted k_{trans} by a factor of two for each dyad. The result would be a good match between calculated and measured rates for all dyads except for **Dyad-6**, which would then be slower than predicted by about a factor of two (for reasons unknown). For reference, the average edge-to-edge distance between donor and acceptor bacteriochlorins spaced by the phenylethyne linker is 8.4 Å. Thus, a 13.6 Å average distance employed in the Förster calculations for the effective separation

of the donor and acceptor TDMs is not physically unreasonable. Higher level theory that employs transition-density-cubed[77] or other methods would address this issue.

E. Through-bond versus through-space energy transfer. A germane question for the dyads depicted in Chart 1 concerns the nature of the electronic communication between the donor and acceptor bacteriochlorins. The bacteriochlorin–bacteriochlorin interactions could potentially be of three fundamental types. The first is linker-mediated through-bond (TB) coupling of the aromatic π-electron systems of the two constituents. The second and third types entail through-space (TS) interactions albeit by distinct means. Short-range TS coupling stems from direct π-π overlap of the MOs on the two bacteriochlorins. Longer-range TS interactions originate from coupling of the transition-dipole moments (i.e., dipole-dipole coupling) on the donor and acceptor subunits. The TB and short-range π-π TS interactions are ground-state in nature and give rise to linear-combination MOs, MO splitting, split redox waves and excited states with characteristics of the two components.[78-80] The longer-range dipole-dipole coupling is excited-state in nature and does not afford the linear-combination MOs or split redox waves characteristic of ground-state interactions. In the following, the linker-mediated interactions are referred to as TB, the long-range dipole-dipole coupling as TS, and the short-range (through-space) interactions as direct π-π overlap.

In the present dyads, the two bacteriochlorins joined via the phenylethyne linker are essentially perpendicular to one another (*vide supra*). The result is (1) negligible TB interaction of the two macrocycles and (2) negligible direct π–π overlap between the two macrocycles. Thus, the donor–acceptor electronic interactions are dominated by the TS resonant coupling of the TDMs of the two bacteriochlorins. For energy transfer, the relevant TDMS are for the $S_1 \rightarrow S_0$ fluorescence of the donor and the $S_0 \rightarrow S_1$ absorption TDM for the acceptor. Of course, the rate

constants and dipole-strengths for the absorption and fluorescence transitions on each unit are connected by the relationships between the Einstein coefficients.[81,82]

F. Calculated molecular orbital and spectral properties. DFT calculations were performed to obtain the energies and electron-density distributions of the frontier MOs of the benchmark donor monomers, benchmark acceptor monomers, and the dyads. In general, the frontier MOs of the bacteriochlorin monomers are similar to the familiar orbitals of Gouterman's four-orbital model.[83-86] The MOs of the dyads are comprised of the sets of orbitals expected from the donor and acceptor monomers and are presented in Tables S3–S11.

TDDFT calculations were carried out to obtain spectral and excited-state properties for the monomers and dyads. The derived properties include the electronic compositions of the excited states responsible for the visible and NIR absorption spectra, and the associated $S_0 \rightarrow S_n$ (n = 1–16) transition energies and oscillator strengths (f). The S_1 excited state of each bacteriochlorin monomer, as expected, is comprised of the ~90% $a_{1u}(\pi) \rightarrow e_{gx}(\pi^*)$ and ~10% $a_{2u}(\pi) \rightarrow e_{gy}(\pi^*)$ configurations within the four-orbital model. These results for the dyads are given in Tables S1 and S12–S20. These calculations also show, as is expected within the four-orbital model, that each excited state is comprised of two or more excited-state configurations involving one-electron promotions between filled and empty frontier MOs. The NTOs were also obtained to help visualize the electron-density changes that occur in making a transition from the ground state to a given excited state.[87] Each electronic excitation is viewed as a set of one-electron promotions from a filled NTO to an empty NTO with different relative weights. The filled and empty NTOs for a given transition are referred to here as an NTO pair. Full sets of NTOs for transitions from S_0 to S_{16} for the dyads are given in Tables S21–S29.

For each dyad, Figures S1–S9 present the measured and calculated absorption spectra spanning the violet and the NIR regions along with the NTO pairs for the $S_0 \rightarrow S_1$ and $S_0 \rightarrow S_2$

transition. These illustrations for **Dyad-1** and **Dyad-9** are presented in Figures 8A and 8B, respectively. Of course, in the dyad, S_2 is the lowest singlet excited state of the donor bacteriochlorin, and S_1 is the lowest singlet excited state of the acceptor bacteriochlorin. The calculated wavelengths/energies of the S_2 and S_1 excited states and the associated wavelength/energy gap for all nine dyads are collected in Table S1. The wavelength and energy gaps for the dyads are also given in the last column of Table 4. One can see the good agreement between the donor–acceptor energy gaps that were (1) measured for the dyads, (2) calculated by TDDFT, and (3) predicted from substituent effects on spectra of reference bacteriochlorins as part of the design of the set of nine dyads.

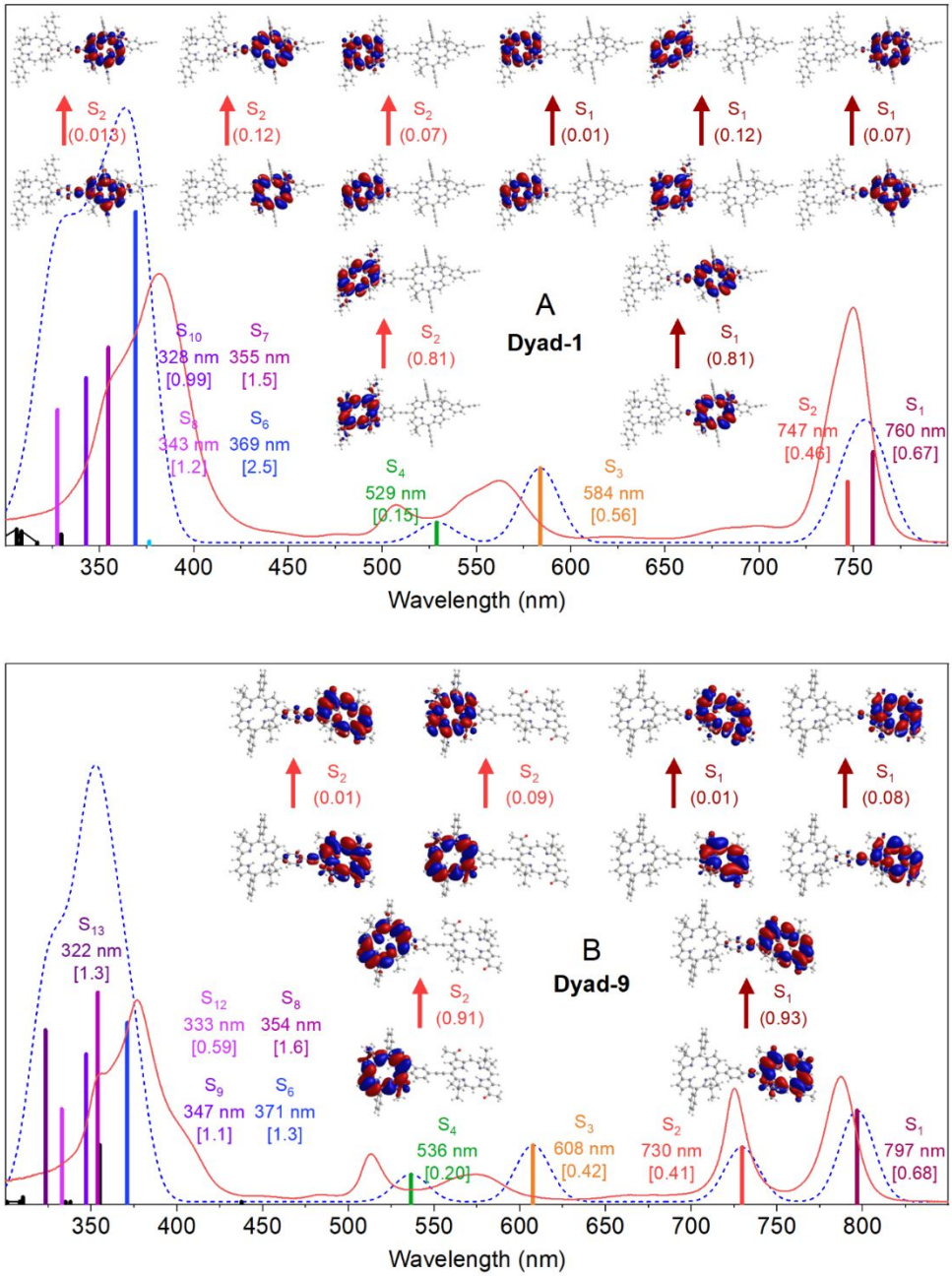

Figure 8. Absorption spectra measured (red) and calculated by TDDFT (colored sticks and blue dashed lines using 10-nm Gaussian skirts) for **Dyad-1** (A) and **Dyad-9** (B) in toluene. The $S_0 \rightarrow S_1$ and $S_0 \rightarrow S_2$ transitions both have multiple pairs of occupied and virtual NTOs with relative weights indicated in parenthesis. The calculated wavelength and oscillator strength (in square brackets) for each transition are given at the bottom of each panel.

An exact match is not expected for the donor–acceptor excited-state energies (and Q_y wavelength spacing) measured in the dyads with the values predicted from the monomers. This is so because donor–acceptor electronic interactions in the dyad will add to the splitting of the exited-

state energies relative to the spacing in the monomers. In this regard, we utilized the transition-dipole-moment vectors and relative orientations coordinates from the TDDFT calculations to estimate the dipole–dipole coupling energy for each dyad.[47] The values are in the range 42–67 cm^{-1} with an average of 55 cm^{-1}. For perspective, a splitting of twice this interaction energy would correspond to a spectral splitting of 5 nm at 700 nm. Such a difference in relative donor and acceptor Q_y bands compared to those of the benchmark monomers cannot be reliably seen in the spectra. Each benchmark monomer does not contain all the atoms of the linker that each bacteriochlorin experiences in the dyad. Furthermore, in the dyad, steric interactions may influence the precise orientation of the phenyl group of the linker and the donor bacteriochlorin compared to the positioning in the donor monomer.

Turning to Figure 8, the spectra calculated by TDDFT reproduce the major characteristics of the measured spectra for the dyads, including the $S_2 - S_1$ wavelength/energy spacing noted above. Close examination of the NTO pairs and their relative weighting for the S_2 and S_1 states provide additional insights into factors that contribute to excited-state energy transfer. The S_1 excited state of **Dyad-1** is comprised of two NTO pairs that have electron density on the donor with eigenvalues that contribute 87% of the total and two pairs on the acceptor that together afford 13% (Figure 8A). These results suggest that 87% of the character of the S_1 excited state of **Dyad-1** is associated with the acceptor and roughly 13% with the donor. Complementary to that, the NTO pairs for the S_2 state of **Dyad-1** have net 87% weighting on the donor and 13% on the acceptor. Turning to **Dyad-9** (Figure 8B), the three NTO pairs for S_1 are 100% on the acceptor and two of the three NTO pairs for S_2 are on the donor and give a dominant 99% weighting.

The NTO characteristics for the S_1 and S_2 states for all dyads are summarized in Table S2. Figure 4E captures these results by plotting the fraction of the S_1 state associated with the donor bacteriochlorin as a function of donor–acceptor excited-state energy gap. As the energy gap

increases, the amount of donor excited-state character mixed in with the dominant acceptor character of the S_1 state decreases. The extent of quantum-mechanical mixing decreases with increasing energy gap due to a smaller energy denominator. A related observation (described above concerning Figure 3C) is that a small amount of the total fluorescence appears to arise from the S_2 state of **Dyad-1** (i.e., the donor bacteriochlorin), which apparently decreases as the donor–acceptor excited-state energy gap increases. This result may also originate from quantum mechanical as well as thermal mixing of the two lowest singlet excited states of the dyad.

The contribution of transitions (and NTOs) on the donor to the character of the S_1 state must inevitably derive from electronic interactions between the donor and acceptor bacteriochlorins. Although the TDDFT calculations do not explicitly utilize the coupling of TDMs of the donor and acceptor constituents, the method obviously incorporates interaction of donor and acceptor wavefunctions. Both methods have a dependence on relative donor–acceptor energetics, such as energy denominators for electronic mixing in the TDDFT calculations and spectral overlap in the Förster calculations of the energy-transfer rate. Such connections likely underlie the overall similar trends with donor–acceptor excited-state energy gap of (1) the donor character mixed into S_1 suggested by the TDDFT calculations (Figure 4E), (2) the spectral overlap integral J in the Förster calculations (Figure 4C) and (3) the measured rate constant for excited-state energy transfer (Figure 4A).

Conclusions

Nine phenylethynyl-linked bacteriochlorin dyads spanning a range of donor–acceptor energy gaps (~200–1100 cm^{-1}) were synthesized. The phenylethynyl linker (1) is an unsymmetric auxochrome that imparts a substantial bathochromic shift ($\Delta\lambda$ ~22 nm) of the Q_y band of the ethyne-attached bacteriochlorin but relatively little shift ($\Delta\lambda$ ~5 nm) of the phenyl-attached

bacteriochlorin; (2) provides a distance of separation of the two bacteriochlorins to support ultrafast energy transfer $(0.3–1.7\ ps)^{-1}$; and (3) is compatible with the constraints of extant synthesis methodology for gem-dimethyl-substituted bacteriochlorins. The rate of energy transfer for each dyad is consistent with the prediction using Förster theory within a factor of two. The orientation parameter in the Förster process has been analyzed in depth for the covalently linked dyads, taking into account the substituent-induced disposition of the TDM in each bacteriochlorin. In general, each TDM has been found to be slightly out-of-plane and non-coincident with the NH–NH axis of the substituted bacteriochlorin macrocycle. The ability to tune the wavelength to alter NIR light-harvesting while maintaining supremely fast and efficient energy transfer augurs well for studies in artificial photosynthesis and potential use in diverse applications (solar light-harvesting, clinical diagnostics, biosensors, etc.) where FRET processes are germane.

Experimental section

General methods

^{1}H NMR and ^{13}C NMR spectra were collected at room temperature in $CDCl_3$ unless noted otherwise. Silica (40 μm average particle size) was used for column chromatography. THF was freshly distilled from sodium/benzophenone. All other solvents (anhydrous or reagent-grade) were employed as received from commercial suppliers. Electrospray ionization mass spectrometry (ESI-MS) data generally enable accurate mass measurements and were obtained in the positive-ion mode. Commercial compounds were used as received. The bacteriochlorin building block **Br-BC-5** was prepared as described by Chakraborty *et al*.,[64] whereas all others (**BC-1**, **BC-2**, **BC-3**, **BC-4**, **Br-BC-6**, **Br-BC-7**, **Br-BC-8**, **Br-BC-9**) we described previously.[62]

Typical procedure for purification of dyads

After the completion of the reaction, the reaction mixture was allowed to cool to room temperature and then concentrated *in vacuo*. The resulting crude mixture was chromatographed on silica to remove palladium reagents, phosphine ligands and derived species, and other undesired entities. The collected eluant was further purified by preparative SEC (Bio-beads S-X1, 200–400 mesh,

toluene) to remove bacteriochlorin monomers and oligomers. The eluant collected from SEC was passed through a short silica pad to remove residues that leach from the SEC polymer beads, thereby affording the pure bacteriochlorin monomer or dyad.

Synthetic procedures

15-(4-Ethynylphenyl)-5-{2-[4-(2,12-bis(4-methylphenyl)-8,8,18,18-tetramethylbacteriochlorin-5-yl)phenyl]ethynyl}-10,20-diphenyl-8,8,18,18-tetramethylbacteriochlorin (Dyad-1). A solution of **Br-BC-9** (1.5 mg, 1.7 μmol), **BC-3** (1.4 mg, 2.2 μmol) and P(*o*-tol)$_3$ (5.2 mg, 17 μmol) in toluene/TEA (2.1 mL, 5:1) was degassed by freeze/pump/thaw cycles (4 times). A sample of $Pd_2(dba)_3$ (2.2 mg, 1.9 μmol) was then added, and the resulting mixture was stirred for 14 h at 70 °C. The mixture was allowed to cool to room temperature, and then concentrated and chromatographed [silica, hexanes/CH_2Cl_2 (2:1 to 1:1)]. The resulting crude product was dissolved in THF (3.0 mL) and treated with TBAF/THF (1.0 M, 10 μL, 10 μmol) at room temperature for 3 h. Then CH_2Cl_2 and water were added. The organic layer was dried (Na_2SO_4), concentrated and chromatographed [silica, hexanes/CH_2Cl_2 (2:1 to 1:1)]. The resulting crude with further purified by SEC (toluene; one passage) followed by a short silica pad to afford a pink solid (0.8 mg, 36%). A quality ^{1}H NMR spectrum was not obtained in $CDCl_3$ or CD_2Cl_2 due to limited solubility. ESI-MS obsd 635.3163, calcd 635.3169 [$(M)^{2+}$, M = $C_{90}H_{78}N_8$]; λ_{abs} (toluene) 383, 508, 562, 699, 750 nm.

5-{2-[4-(15-(4-Formylphenyl)-10,20-diphenyl-8,8,18,18-tetramethylbacteriochlorin-5-yl)phenyl]ethynyl}-10,20-diphenyl-8,8,18,18-tetramethylbacteriochlorin (Dyad-2). A solution of **Br-BC-5** (1.3 mg, 1.7 μmol) and **BC-2** (1.0 mg, 1.4 μmol) in toluene/TEA (1.8 mL, 5:1) was and P(*o*-tol)$_3$ (3.3 mg, 11 μmol) in toluene/TEA (1.8 mL, 5:1) was degassed by freeze/pump/thaw cycles (5 times). A sample of $Pd_2(dba)_3$ (4.3 mg, 4.7 μmol) was then added, and the resulting mixture was stirred for 15 h at 70 °C. The mixture was allowed to cool to room temperature, and then concentrated and chromatographed [silica, hexanes/CH_2Cl_2 (2:1 to 1:2)]. The resulting crude product was further purified by SEC (toluene; one passage) followed by a short silica pad to afford a pink-purple solid (1.2 mg, 70%): ^{1}H NMR (700 MHz, CD_2Cl_2) δ −1.57 (s, 1H), −1.55 (s, 1H), −1.35 (s, 1H), −1.26 (s, 1H), 1.33 (s, 6H), 1.36 (s, 6H), 1.46 (s, 6H), 1.53 (s, 6H), 3.80 (s, 2H), 3.94 (s, 2H), 4.28 (s, 2H), 4.68 (s, 2H), 7.48–7.52 (m, 3H), 7.53–7.57 (m, 6H), 7.59–7.63 (m, 3H), 7.70–7.73 (m, 1H), 7.59–7.63 (m, 3H), 7.76–7.78 (m, 1H), 7.79–7.83 (m, 5H), 7.83–7.88 (m, 8H), 7.94 (d, J = 7.8 Hz, 2H), 7.98–8.01 (m, 1H), 8.06 (d, J = 7.8 Hz, 2H),

8.07–8.10 (m, 2H), 8.46 (s, 1H), 8.70 (s, 1H), 9.13 (s, 1H), 10.18 (s, 1H); ESI-MS obsd 1247.6020, calcd 1247.6058 [$(M + H)^+$, M = $C_{87}H_{74}N_8O$]; λ_{abs} (toluene) 381, 523, 553, 731, 745 nm.

2,12-Diethoxycarbonyl-5-{2-[4-(2,12-diethoxycarbonyl-8,8,18,18-tetramethylbacteriochlorin-5-yl)phenyl]ethynyl}-8,8,18,18-tetramethylbacteriochlorin (Dyad-3). A solution of **Br-BC-7** (2.0 mg, 3.3 μmol) and **BC-4** (1.8 mg, 2.9 μmol) in toluene/TEA (2.4 mL, 5:1) was degassed by freeze/pump/thaw cycles (4 times). A sample of $Pd(PPh_3)_4$ (2.7 mg, 2.3 μmol) was then added, and the resulting mixture was stirred for 16 h at 70 °C. The mixture was allowed to cool to room temperature, and then concentrated and chromatographed [silica, hexanes/CH_2Cl_2 (1:1 to 0:1)]. The resulting crude product was further purified by SEC (toluene; one passage) followed by a short silica pad to afford a purple solid (1.8 mg, 54%): ^{1}H NMR (700 MHz) δ −1.23 (s, 1H), −1.12 (s, 1H), −0.98 (s, 1H), −0.86 (s, 1H), 1.66 (t, J = 7.2 Hz, 3H), 1.72 (t, J = 7.2 Hz, 6H), 1.76 (t, J = 7.2 Hz, 3H), 1.95 (s, 6H), 1.995 (s, 6H), 2.004 (s, 6H), 2.03 (s, 6H), 4.08 (s, 2H), 4.36 (s, 2H), 4.40 (s, 2H), 4.72 (q, J = 7.2 Hz, 2H), 4.73 (s, 2H), 4.78 (q, J = 7.2 Hz, 4H), 4.82 (q, J = 7.2 Hz, 2H), 8.01 (d, J = 7.8 Hz, 2H), 8.27 (d, J = 7.6 Hz, 2H), 8.70 (s, 1H), 8.72–8.75 (m, 2H), 9.16 (d, J = 2.1 Hz, 1H), 9.21 (d, J = 2.1 Hz, 1H), 9.73 (s, 1H), 9.75 (d, J = 2.2 Hz, 1H), 9.80 (s, 1H), 9.83 (s, 1H); ^{13}C{^{1}H} NMR (175 MHz) δ 14.7, 14.8, 14.9, 31.0, 31.06, 31.08, 31.4, 45.9, 46.1, 46.19, 46.21, 51.1, 51.2, 51.3, 51.9, 60.9, 61.00, 61.02, 92.3, 96.6, 96.7, 97.6, 98.0, 98.1, 99.0, 100.5, 101.5, 115.3, 121.5, 122.0, 123.1, 123.2, 123.4, 124.6, 125.1, 126.4, 126.5, 131.3, 132.4, 133.6, 134.0, 134.2, 134.4, 135.59, 135.64, 136.2, 136.4, 142.6, 159.0, 161.0, 161.2, 164.0, 165.4, 165.5, 165.76, 165.79, 172.4, 172.6, 173.4, 174.0; ESI-MS obsd 1126.5290, calcd 1126.5311 [$(M)^+$, M = $C_{68}H_{70}N_8O_8$]; λ_{abs} (toluene) 358, 382, 534, 573, 757, 775 nm.

15-(4-Ethynylphenyl)-5-{2-[4-(15-(4-formylphenyl)-10,20-diphenyl-8,8,18,18-tetramethylbacteriochlorin-5-yl)phenyl]ethynyl}-10,20-diphenyl-8,8,18,18-tetramethylbacteriochlorin (Dyad-4). A solution of **Br-BC-9** (1.5 mg, 1.7 μmol), **BC-2** (1.0 mg, 1.4 μmol) and P(o-tol)$_3$ (7.2 mg, 24 μmol) in toluene/TEA (1.8 mL, 5:1) was degassed by freeze/pump/thaw cycles (4 times). A sample of $Pd_2(dba)_3$ (4.3 mg, 4.7 μmol) was then added, and the resulting mixture was stirred for 15 h at 70 °C. The mixture was allowed to cool to room temperature, and then concentrated and chromatographed [silica, hexanes/CH_2Cl_2 (1:1 to 0:1)]. The resulting crude product was dissolved in THF (2.0 mL) and treated with TBAF/THF (1.0 M, 10 μL, 10 μmol) at room temperature for 3 h. Then CH_2Cl_2 and water were added. The organic layer was dried (Na_2SO_4), concentrated and chromatographed [silica, hexanes/CH_2Cl_2 (2:1 to 0:1)]. The resulting crude with further purified by SEC (toluene; one passage) followed by a short

silica pad to afford a pink solid (1.6 mg, 77%). A quality ^{1}H NMR spectrum could not be obtained in a series of solvents ($CDCl_3$, CD_2Cl_2, THF-d_8, C_6D_6 and CS_2) due to limited solubility. ESI-MS obsd 1347.6371, calcd 1347.6383 [$(M + H)^+$, M = $C_{95}H_{78}N_8O$]; λ_{abs} (toluene) 383, 524, 561, 731, 750 nm.

5-{2-[4-(10,20-Diphenyl-8,8,18,18-tetramethylbacteriochlorin-5-yl)phenyl]ethynyl}-10,20-diphenyl-8,8,18,18-tetramethylbacteriochlorin (Dyad-5). A solution of **Br-BC-5** (3.5 mg, 5.8 μmol), **BC-1** (3.0 mg, 4.8 μmol) and P(*o*-tol)$_3$ (8.1 mg, 26.6 μmol) in toluene/TEA (3.0 mL, 5:1) was degassed by freeze/pump/thaw cycles (4 times). A sample of $Pd_2(dba)_3$ (3.2 mg, 3.5 μmol) was then added, and the resulting mixture was stirred for 22 h at 60 °C. The mixture was allowed to cool to room temperature, and then concentrated and chromatographed [silica, hexanes/CH_2Cl_2 (1:1)]. The resulting crude product was further purified by SEC (toluene; one passage) followed by a short silica pad to afford a pink purple solid (3.5 mg, 65%): ^{1}H NMR (700 MHz) δ −1.52 (s, 1H), −1.47 (s, 1H), −1.25 (s, 1H), −1.18 (s, 1H), 1.28 (s, 3H), 1.33 (s, 3H), 1.46 (s, 6H), 1.61 (s, 6H), 3.99 (s, 2H), 4.34 (s, 2H), 4.38 (s, 2H), 4.75 (s, 2H), 7.51–7.72 (m, 12H), 7.74–7.93 (m, 11H), 7.96 (d, *J* = 3.3 Hz, 2H), 7.99–8.05 (m, 2H), 8.10 (s, 1H), 8.11 (s, 1H), 8.50 (d, *J* = 2.6 Hz, 1H), 8.55 (d, *J* = 3.1 Hz, 1H), 8.75 (s, 1H), 8.77 (s, 1H), 9.21 (dd, *J* = 4.1, 1.4 Hz, 1H); a quality ^{13}C NMR spectrum could not be obtained due to limited solubility; ESI-MS obsd 1142.5676, calcd 1142.5718 [$(M)^+$, M = $C_{80}H_{70}N_8$]; λ_{abs} (toluene) 378, 514, 555, 726, 744 nm.

2,12-Bis(4-methylphenyl)-5-{2-[4-(10,20-diphenyl-8,8,18,18-tetramethylbacteriochlorin-5-yl)phenyl]ethynyl}-8,8,18,18-tetramethylbacteriochlorin (Dyad-6). A solution of **Br-BC-6** (1.1 mg, 1.7 μmol) and **BC-1** (1.0 mg, 1.6 μmol) in toluene/TEA (1.8 mL, 5:1) was degassed by freeze/pump/thaw cycles (4 times). A sample of $Pd(PPh_3)_4$ (2.2 mg, 1.9 μmol) was then added, and the resulting mixture was stirred for 12 h at 70 °C. The mixture was allowed to cool to room temperature, and then concentrated and chromatographed [silica, hexanes/CH_2Cl_2 (2:1)]. The resulting crude product was further purified by SEC (toluene; one passage) followed by a short silica pad to afford a pink solid (1.1 mg, 58%): ^{1}H NMR (700 MHz, CD_2Cl_2) δ −1.51 (s, 1H), −1.49 (s, 1H), −1.45 (s, 1H), −1.39 (s, 1H), 1.52 (s, 6H), 1.59 (s, 6H), 1.97 (s, 6H), 2.03 (s, 6H), 2.64 (s, 3H), 2.65 (s, 3H), 4.07 (s, 2H), 4.45 (s, 2H), 4.49 (s, 2H), 4.83 (s, 2H), 7.60–7.77 (m, 8H), 7.83–7.88 (m, 2H), 7.95 (d, *J* = 8.2 Hz, 1H), 7.97 (d, *J* = 6.8 Hz, 1H), 8.00 (d, *J* = 7.8 Hz, 2H), 8.05–8.11 (m, 2H), 8.17 (d, *J* = 7.7 Hz, 2H), 8.23 (d, *J* = 7.8 Hz, 2H), 8.22–8.27 (m, 2H), 8.59–8.66 (m, 2H), 8.76–8.87 (m, 4H), 8.88–8.96 (m, 3H), 9.35 (s, 1H); ESI-

MS obsd 585.3010, calcd 585.3013 [$(M)^{2+}$, M = $C_{82}H_{74}N_8$]; λ_{abs} (toluene) 378, 514, 545, 725, 760 nm.

2,12-Diethoxycarbonyl-5-{2-[4-(15-(4-formylphenyl)-10,20-diphenyl-8,8,18,18-tetramethylbacteriochlorin-5-yl)phenyl]ethynyl}-8,8,18,18-tetramethylbacteriochlorin (Dyad-7). A solution of **Br-BC-7** (1.0 mg, 1.7 μmol) and **BC-2** (1.0 mg, 1.4 μmol) in toluene/TEA (1.8 mL, 5:1) was degassed by freeze/pump/thaw cycles (4 times). A sample of $Pd(PPh_3)_4$ (2.2 mg, 1.9 μmol) was then added, and the resulting mixture was stirred for 13 h at 70 °C. The mixture was allowed to cool to room temperature, and then concentrated and chromatographed [silica, hexanes/CH_2Cl_2 (1:1 to 0:1)]. The resulting crude product was further purified by SEC (toluene; one passage) followed by a short silica pad to afford a purple solid (1.3 mg, 76%): ^{1}H NMR (700 MHz,) δ −1.57-−1.51 (m, 2H), −1.07 (s, 1H), −0.95 (s, 1H), 1.34 (s, 6H), 1.39 (s, 6H), 1.61 (t, *J* = 7.2 Hz, 3H), 1.63 (t, *J* = 7.2 Hz, 3H), 1.89 (s, 6H), 1.95 (s, 6H), 3.81 (s, 2H), 3.97 (s, 2H), 4.29 (s, 2H), 4.63 (s, 2H), 4.66 (q, *J* = 7.2 Hz, 2H), 4.69 (q, *J* = 7.2 Hz, 2H), 7.49–7.58 (m, 7H), 7.73 (dd, *J* = 4.2, 1.5 Hz, 1H), 7.80 (td, *J* = 4.1, 1.5 Hz, 2H), 7.81–7.84 (m, 3H), 7.93 (d, *J* = 7.6 Hz, 2H), 7.95 (d, *J* = 7.6 Hz, 2H), 8.03 (dd, *J* = 5.5, 1.9 Hz, 1H), 8.09 (d, *J* = 7.5 Hz, 2H), 8.14 (d, *J* = 7.7 Hz, 2H), 8.66 (s, 1H), 9.08-9.10 (m, 1H), 9.60-9.62 (m, 2H), 9.67 (s, 1H), 10.19 (s, 1H); ESI-MS obsd 1239.5862, calcd 1239.5855 [$(M)^+$, M = $C_{81}H_{74}N_8O_5$]; λ_{abs} (toluene) 381, 522, 573, 731, 775 nm.

2,12-Diethoxycarbonyl-5-{2-[4-(10,20-diphenyl-8,8,18,18-tetramethylbacteriochlorin-5-yl)phenyl]ethynyl}-8,8,18,18-tetramethylbacteriochlorin (Dyad-8). A solution of **Br-BC-7** (2.0 mg, 3.3 μmol) and **BC-1** (1.9 mg, 3.1 μmol) in toluene/TEA (1.8 mL, 5:1) was degassed by freeze/pump/thaw cycles (4 times). A sample of $Pd(PPh_3)_4$ (4.2 mg, 3.5 μmol) was then added, and the resulting mixture was stirred for 18 h at 70 °C. The mixture was allowed to cool to room temperature, and then concentrated and chromatographed [silica, hexanes/CH_2Cl_2 (1:1)]. The resulting crude product was further purified by SEC (toluene; one passage) followed by a short silica pad to afford a purple solid (3.4 mg, 90%): ^{1}H NMR (700 MHz) δ −1.50 (s, 1H), −1.44 (s, 1H), −1.00 (s, 1H), −0.89 (s, 1H), 1.49 (s, 6H), 1.55 (s, 6H), 1.71 (t, *J* = 7.2 Hz, 3H), 1.74 (t, *J* = 7.2 Hz, 3H), 1.98 (s, 6H), 2.03 (s, 6H), 4.02 (s, 2H), 4.35 (s, 2H), 4.40 (s, 2H), 4.69 (s, 2H), 4.77 (q, *J* = 7.2 Hz, 2H), 4.78 (q, *J* = 7.2 Hz, 2H), 7.52–7.72 (m, 7H), 7.82–7.85 (m, 1H), 7.89–7.94 (m, 3H), 7.94–8.00 (m, 3H), 8.03–8.07 (m, 1H), 8.17–8.22 (m, 2H), 8.56 (d, *J* = 3.3 Hz, 1H), 8.69 (s, 1H), 8.79 (s, 1H), 9.15 (s, 1H), 9.68–9.73 (m, 2H), 9.78 (s, 1H); ^{13}C{^{1}H} NMR (175 MHz) δ14.7, 14.8, 30.0, 30.1, 31.0, 31.4, 45.9, 46.2, 47.1, 47.2, 51.1, 51.9, 55.4, 55.5,

60.98, 60.99, 91.9, 96.8, 97.9, 98.9, 99.4, 101.4, 114.2, 114.6, 115.6, 121.7, 121.8, 122.0, 122.8, 122.9, 123.0, 123.8, 124.7, 126.3, 126.4, 127.5, 127.6, 131.0, 132.3, 133.7, 133.8, 134.0, 134.4, 134.9, 135.6, 135.9, 136.4, 138.1, 139.3, 140.9, 141.0, 144.9, 155.2, 157.8, 160.9, 164.0, 165.4, 165.7, 166.1, 167.9, 172.6, 173.9; ESI-MS obsd 1134.5520, calcd 1134.5520 [$(M)^+$, M = $C_{74}H_{70}N_8O_4$], (strong peaks at *m/z* = 523.3251 and 614.2894 also were observed, consistent with cleavage preferentially between the diphenylbacteriochlorin unit and the linker); λ_{abs} (toluene) 378, 513, 572, 726, 775 nm.

2,12-Diacetyl-5-{2-[4-(10,20-diphenyl-8,8,18,18-tetramethylbacteriochlorin-5-yl)phenyl]ethynyl}-8,8,18,18-tetramethylbacteriochlorin (Dyad-9). A solution of **Br-BC-8** (1.0 mg, 1.9 μmol) and **BC-1** (1.0 mg, 1.6 μmol) in toluene/TEA (1.8 mL, 5:1) was degassed by freeze/pump/thaw cycles (4 times). A sample of $Pd(PPh_3)_4$ (2.5 mg, 2.2 μmol) was then added, and the resulting mixture was stirred for 16 h at 70 °C. The mixture was allowed to cool to room temperature, and then concentrated and chromatographed (silica, CH_2Cl_2). The resulting crude product was further purified by SEC (toluene; one passage) followed by a short silica pad to afford a purple solid (1.1 mg, 64%): ^{1}H NMR (700 MHz, CD_2Cl_2) δ −1.48 (s, 1H), −1.43 (s, 1H), −0.76 (s, 1H), −0.64 (s, 1H), 1.52 (s, 6H), 1.59 (s, 6H), 2.00 (s, 6H), 2.05 (s, 6H), 3.19 (s, 3H), 3.27 (s, 3H), 4.07 (s, 2H), 4.38 (s, 2H), 4.45 (s, 2H), 4.73 (s, 2H), 7.62–7.68 (m, 4H), 7.68–7.73 (m, 3H), 7.86 (dd, *J* = 4.6, 1.8 Hz,1H), 7.94–7.98 (m, 3H), 8.00 (dd, *J* = 4.6, 1.7 Hz,1H), 8.03 (d, *J* = 7.7 Hz, 2H), 8.07 (dd, *J* = 4.6, 2.1 Hz,1H), 8.25 (d, *J* = 7.7 Hz, 2H), 8.63 (dd, *J* = 4.8, 1.9 Hz,1H), 8.75 (s, 1H), 8.85 (s, 1H), 9.10 (d, *J* = 2.0 Hz, 1H), 9.65 (d, *J* = 2.1 Hz, 1H), 9.77 (s, 1H), 984 (s, 1H); ESI-MS obsd 1075.5387, calcd 1075.5382 [$(M + H)^+$, M = $C_{72}H_{66}N_8O_2$]; λ_{abs} (toluene) 377, 513, 574, 726, 788 nm.

5-(2-Phenylethynyl)-10,20-diphenyl-8,8,18,18-tetramethylbacteriochlorin (PhE-BC-5). A solution of **Br-BC-5** (1.7 mg, 2.8 μmol), phenylacetylene (4.0 μL, 15 μmol) and P(*o*-tol)$_3$ (3.7 mg, 12 μmol) in toluene/TEA (1.8 mL, 5:1) was degassed by freeze/pump/thaw cycles (4 times). A sample of $Pd_2(dba)_3$ (2.7 mg, 2.9 μmol) was then added, and the resulting mixture was stirred for 16 h at 70 °C. The mixture was allowed to cool to room temperature, and then concentrated and chromatographed [silica, hexanes/CH_2Cl_2 (6:1 to 3:1)]. The resulting crude product was further purified by SEC (toluene; five passages) followed by a short silica pad to afford a red-purple solid (0.9 mg, 51%): ^{1}H NMR (500 MHz) δ −1.30 (s, 1H), −1.25 (s, 1H), 1.52 (s, 6H), 1.56 (s, 6H), 1.55 (s, 12H), 4.33 (s, 2H), 4.63 (s, 2H), 7.38–7.51 (m, 5H), 7.56–7.68 (m, 6H), 7.82–7.92 (m, 6H), 8.49 (dd, *J* = 4.6, 1.9 Hz, 1H), 8.73 (s, 1H), 9.08 (dd, *J* = 4.6, 2.1 Hz, 1H);

$^{13}C\{^{1}H\}$ NMR (175 MHz) δ 11.4, 18.8, 29.9, 30.1, 41.1, 50.9, 55.3, 55.4, 91.0, 99.4, 107.3, 114.1, 114.6, 115.5, 121.6, 121.8, 122.3, 123.7, 126.29, 126.34, 127.5, 127.6, 131.5, 131.9, 133.7, 133.8, 134.8, 135.8, 138.0, 139.2, 140.9, 141.0, 144.8, 155.1, 157.7, 166.1, 167.7; ESI-MS obsd 622.3096, calcd 622.3091 [$(M)^+$, M = $C_{44}H_{38}N_4$]; λ_{abs} (toluene) 376, 548, 743 nm.

2,12-Bis(4-methylphenyl)-5-(2-phenylethynyl)-8,8,18,18-tetramethylbacteriochlorin (PhE-BC-6). A solution of **Br-BC-6** (1.0 mg, 1.6 μmol) and phenylacetylene (4.0 μL, 15 μmol) in toluene/TEA (1.2 mL, 5:1) was degassed by freeze/pump/thaw cycles (4 times). A sample of $Pd(PPh_3)_4$ (2.3 mg, 2.0 μmol) was then added, and the resulting mixture was stirred for 14 h at 70 °C. The mixture was allowed to cool to room temperature, and then concentrated and chromatographed [silica, hexanes/CH_2Cl_2 (3:1 to 2:1)]. The resulting crude product was further purified by SEC (toluene; three passages) followed by a short silica pad to afford a pink-red solid (0.7 mg, 68%): ^{1}H NMR (700 MHz) δ −1.59 (s, 1H), −1.50 (s, 1H), 1.91 (s, 6H), 1.94 (s, 6H), 2.60–2.62 (m, 6H), 4.40 (s, 2H), 4.66 (s, 2H), 7.42–7.46 (m, 1H), 7.49–7.53 (m, 2H), 7.56–7.60 (m, 4H), 7.91 (d, J = 6.6 Hz, 2H), 8.10 (d, J = 7.7 Hz, 2H), 8.13 (d, J = 7.8 Hz, 2H), 8.68 (d, J = 2.0 Hz, 1H), 8.74 (s, 1H), 8.81 (s, 1H), 8.84 (s, 1H), 9.19 (d, J = 2.1 Hz, 1H); $^{13}C\{^{1}H\}$ NMR (175 MHz) δ 21.4, 30.9, 31.3, 45.7, 46.1, 51.3, 52.0, 92.3, 94.4, 95.2, 96.0, 97.0, 99.4, 119.7, 120.7, 124.5, 125.3, 128.0, 128.2, 128.6, 129.0, 129.7, 129.8, 130.9, 131.1, 131.5, 133.5, 133.6, 133.9, 134.5, 134.8, 135.4, 135.8, 136.4, 137.1, 137.3, 158.6, 161.6, 169.8, 171.1 ESI-MS obsd 650.3397, calcd 650.3404 [$(M)^+$, M = $C_{46}H_{42}N_4$]; λ_{abs} (CH_2Cl_2) 370, 538, 756 nm.

2,12-Diethoxycarbonyl-5-(2-phenylethynyl)-8,8,18,18-tetramethylbacteriochlorin (PhE-BC-7). A solution of **Br-BC-7** (2.0 mg, 3.4 μmol) and phenylacetylene (5.0 μL, 19 μmol) in toluene/TEA (1.8 mL, 5:1) was degassed by freeze/pump/thaw cycles (4 times). A sample of $Pd(PPh_3)_4$ (2.5 mg, 2.2 μmol) was then added, and the resulting mixture was stirred for 17 h at 70 °C. The mixture was allowed to cool to room temperature, and then concentrated and chromatographed [silica, hexanes/CH_2Cl_2 (1:1 to 0:1)]. The resulting crude product was further purified by SEC (toluene; one passage) followed by a short silica pad to afford a violet solid (2.0 mg, 96%): ^{1}H NMR (700 MHz) δ −1.05 (s, 1H), −0.96 (s, 1H), 1.70 (t, J = 7.2 Hz, 3H), 1.72 (t, J = 7.2 Hz, 3H), 1.96 (s, 6H), 1.98 (s, 6H), 4.33 (s, 2H), 4.57 (d, J = 1.8 Hz, 2H), 4.75 (q, J = 7.2 Hz, 2H), 4.78 (q, J = 7.2 Hz, 2H), 7.46–7.49 (m, 1H), 7.52–7.56 (m, 2H), 7.92–7.94 (m, 2H), 8.70 (s, 1H), 9.13 (d, J = 2.2 Hz, 1H), 9.59 (d, J = 2.3 Hz, 1H), 9.71 (s, 1H), 9.77 (s, 1H); $^{13}C\{^{1}H\}$ NMR (175 MHz) δ 14.7, 14.8, 31.0, 31.4, 45.8, 46.2, 51.1, 51.8, 60.9, 61.0, 91.4, 96.6, 96.7, 97.9, 98.8, 101.4, 121.9, 123.0, 124.1, 124.6, 126.4, 128.4, 128.7, 131.6, 133.9, 134.3, 135.5, 136.3, 160.9,

163.9, 165.4, 165.7, 172.5, 173.9; ESI-MS obsd 614.2884, calcd 614.2893 [$(M)^+$, M = $C_{38}H_{38}N_4O_4$]; λ_{abs} (toluene) 375, 568, 774 nm.

2,12-Diacetyl-5-(2-phenylethynyl)-8,8,18,18-tetramethylbacteriochlorin (PhE-BC-8). A solution of **Br-BC-8** (1.0 mg, 1.9 μmol), phenylacetylene (10.0 μL, 37.5 μmol) and P(*o*-tol)$_3$ (4.1 mg, 13 μmol) in toluene/TEA (1.2 mL, 5:1) was degassed by freeze/pump/thaw cycles (4 times). A sample of $Pd_2(dba)_3$ (2.4 mg, 2.6 μmol) was then added, and the resulting mixture was stirred for 17 h at 70 °C. The mixture was allowed to cool to room temperature, and then concentrated and chromatographed [silica, hexanes/CH_2Cl_2 (1:1) to CH_2Cl_2]. The resulting crude product was further purified by SEC (toluene; five passages) followed by a short silica pad to afford a dark-purple solid (0.6 mg, 58%): ^{1}H NMR (700 MHz, CD_2Cl_2) δ −0.93 (s, 1H), −0.82 (s, 1H), 1.86 (s, 6H), 1.88 (s, 6H), 3.05 (s, 3H), 3.10 (s, 3H), 4.25 (s, 2H), 4.49 (s, 2H), 7.40–7.43 (m, 1H), 7.46–7.49 (m, 2H), 7.84–7.87 (m, 2H), 8.61 (s, 1H), 8.97 (s, 1H), 9.40 (s, 1H), 9.62 (s, 1H), 9.69 (s, 1H); ^{13}C{^{1}H} NMR (175 MHz, CD_2Cl_2) δ 29.5, 30.6, 31.0, 45.8, 46.0, 51.0, 51.6, 91.1, 96.5, 96.6, 98.8, 99.9, 101.4, 123.9, 124.0, 126.5, 128.4, 128.5, 128.7, 129.8, 131.5, 134.1, 134.3, 134.9, 136.0, 161.5, 164.0, 173.4, 175.1, 196.3, 196.6; ESI-MS obsd 554.2662, calcd 554.2676 [$(M + H)^+$, M = $C_{36}H_{34}N_4O_2$]; λ_{abs} (toluene) 380, 572, 786 nm.

Spectroscopy

All spectroscopic and photophysical studies were carried out in toluene at room temperature on dilute (μM) argon-purged samples using methods described previously.[47]

Density Functional Theory Calculations

DFT calculations were performed with either Gaussian 09 version E.01 or Gaussian 16 version C.01 as described previously.[47] In brief, calculations used the PCM model for the arrays in toluene. Geometry optimization and TDDFT calculations performed using Gaussian 16 employed the keyword G09Defaults in order to emulate a Gaussian 09 calculation. Molecular geometries were fully optimized using the hybrid B3LYP functional and the basis set 6-31G*. These calculations used Gaussian defaults with the exception of keyword Int=(Grid=Ultrafine,Acc2E=12). TDDFT calculations used the long-range corrected wB97XD functional and the basis set 6-31++G**. These calculations used Gaussian defaults with the exception of keywords TD (nStates = 16), and Int = (Grid = Ultrafine, Acc2E = 12).

Conflicts of interest

The authors declare no competing interests.

Acknowledgements

This work was funded by the Division of Chemical Sciences, Geosciences, and Biosciences, Office of Basic Energy Sciences of the U.S. Department of the Energy (FG02-05ER15661). Mass spectrometry data were obtained in the Molecular Education, Technology, and Research Innovation Center (METRIC) at NC State University. The time-resolved optical data were acquired in the Ultrafast Laser Facility of the Photosynthetic Antenna Research Center, an Energy Frontier Research Center supported by the U.S. Department of Energy, Office of Science, Office of Basic Energy Sciences, under Award No. DE-SC0001035.

Supplementary Information

The following are available for nine dyads: calculated S_1 and S_2 energies; calculated versus measured spectra and red-region NTOs; MOs; TDDFT results; NTOs; and NMR spectral data.

References

1 D. Mauzerall and N. L. Greenbaum, *Biochim. Biophys. Acta*, 1989, **974**, 119–140.

2 J. Zhou, J. Chen, Y. Ge and Y. Shao, *Nanophotonics*, 2020, **9**, 1855–1875.

3 M. Taniguchi, G. Hu, R. Liu, H. Du and J. S. Lindsey, *Proc. S.P.I.E. BiOS* 2018, **10508**, 1050806.

4 T. Förster, *Faraday Disc.,* 1959, **27**, 7–17.

5 T. Förster, In *Comparative Effects of Radiation*, M. Burton, J. S. Kirby-Smith and J. L. Magee, Eds., John Wiley & Sons, New York, 1960, pp 300–341.

6 T. Förster, In *Modern Quantum Chemistry–Istanbul Lectures, Part III: Action of Light and Organic Crystals,* O. Sinanoglu, Ed., Academic Press, Inc., New York, 1965, pp 93–137.

7 T. Förster, In *Comprehensive Biochemistry*, Vol. 22, M. Florkin and E. H. Stotz, Eds., Elsevier Publishing Co., Amsterdam., 1967, pp 61–80.

8 A. A. Lamola, In *Energy Transfer and Organic Photochemistry*, Vol. XIV, Technique of Organic Chemistry, P. A. Leermakers and A. Weissberger, Eds., Interscience Publishers, New York, 1969, pp 17–132.

9 R. S. Knox, *J. Biomed. Opt.,* 2012, **17**, 011003.

10 J. S. Lindsey, M. Taniguchi, D. F. Bocian and D. Holten, *Chem. Phys. Rev.,* 2021, **2**, 011302.

11 B. W. van der Meer, *Rev. Mol. Biotechnol.,* 2002, **82**, 181–196.

12 F. Wilkinson, In *Advances in Photochemistry*, Vol. 3, W. A. Noyes, Jr., G. S. Hammond and J. N. Pitts, Jr., Eds., Interscience Publishers, New York, 1964, pp 241–268.

13 I. Z. Steinberg, *Ann. Rev. Biochem*., 1971, **40**, 83–114.

14 L. Stryer, *Ann. Rev. Biochem*., 1978, **47***,* 819–846.

15 P. Wu and L. Brand, *Anal. Biochem.,* 1994, **218**, 1–13.

16 J. Szöllosi, S. Damjanovich and L. Mátyus, *Cytometry,* 1998, **34**, 159–179.

17 K. E. Sapsford, L. Berti and I. L. Medintz, *Angew. Chem. Int. Ed.,* 2006, **45**, 4562–4588.

18 S. S. Vogel, C. Thaler and S. V. Koushik, *Science's STKE,* 2006, **311**, re2.

19 A. Roda, G. Guardigli, E. Michelini and M. Mirasoli, *Anal. Bioanal. Chem*., 2009, **393**, 109–123.

20 A. P. Demchenko, *J. Fluoresc*., 2010, **20**, 1099–1128.

21 H. Sahoo, *J. Photochem. Photobiol. C: Photochem. Rev.,* 2011, **12**, 20–30.

22 S. Preus and L. M. Wilhelmsson, *ChemBioChem,* 2012, **13**, 1990–2001.

23 S. Zadran, S. Standley, K. Wong, E. Otiniano, A. Amighi and M. Baudry, *Appl. Microbiol, Biotechnol.,* 2012, **96**, 895–902.

24 S. Preus, K. Kilså, F.-A. Miannay, B. Albinsson and L. M. Wilhelmsson, *Nucleic Acids Res.,* 2013, **41**, e18.

25 B. R. Masters, *Eur. Phys. J. H,* 2014, **39**, 87–139.

26 S. A. Diaz, D. A. Hastman, I. L. Medintz and E. Oh, *J. Mater. Chem. B,* 2017, **5**, 7907–7926.

27 C. E. Rowland, J. B. Delehanty, C. L. Dwyer and I. L. Medintz, *Mater. Today,* 2017, **20**, 131–141.

28 Q. Qi, M. Taniguchi and J. S. Lindsey, *J. Chem. Inf. Model.,* 2019, **59**, 652–667.

29 J. M. Womick and A. M. Moran, *J. Phys. Chem. B*, 2011, **115**, 1347–1356.

30 A. Kolli, E. J. O'Reilly, G. D. Scholes and A. Olaya-Castro, *J. Chem. Phys.,* 2012, **137**, 174109.

31 N. Christensson, H. F. Kauffmann, T. Pullerits and T. Mančal, *J. Phys. Chem. B*, 2012, **116**, 7449–7454.

32 S. Westenhoff, D. Paleček, P. Edlund, P. Smith and D. Zigmantas, *J. Am. Chem. Soc.,* 2012, **134**, 16484–16487.

33 V. Tiwari, W. K. Peters and D. M. Jonas, *Proc. Natl. Acad. Sci. USA,* 2013, **110**, 1203–1208.

34 A. Chenu, N. Christensson, H. F. Kauffmann and T. Mančal, *Sci. Rep.,* 2013, **3**, 2029.

35 F. D. Fuller, J. Pan, A. Gelzinis, V. Butkus, S. S. Senlik, D. E. Wilcox, C. F. Yocum, L. Valkunas, D. Abramavicius and J. P. Ogilvie, *Nature Chem.,* 2014, **6**, 706–711.

36 I. S. Ryu, H. Dong and G. R. Fleming, *J. Phys. Chem. B*, 2014, **118**, 1381–1388.

37 E. Romero, R. Augulis, V. I. Novoderezhkin, M. Ferretti, J. Thieme, D. Zigmantas and R. van Grondelle, *Nature Phys.,* 2014, **10**, 676–682.

38 M. L. Flanagan, P. D. Long, P. D. Dahlberg, B. S. Rolczynski, S. C. Massey and G. S. Engel, *J. Phys. Chem. A*, 2016, **120**, 1479–1487.

39 V. Tiwari, W. K. Peters and D. M. Jonas, *J. Chem. Phys.,* 2017, **147**, 154308.

40 D. Paleček, P. Edlund, S. Westenhoff and D. Zigmantas, *Sci. Adv.,* 2017, **3**, 1–18.

41 E. Romero, V. I. Novoderezhkin and R. van Grondelle, *Nature,* 2017, **543**, 355–365.

42 Y. Fujihashi, M. Higashi and A. Ishizaki, *J. Phys. Chem. Lett.,* 2018, **9**, 4921–4929.

43 J. Cao, R. J. Cogdell, D. F. Coker, H.-G. Duan, J. Hauer, U. Kleinekathöfer, T. L. C. Jansen, T. Mančal, R. J. D. Miller, J. P. Ogilvie, V. I. Prokhorenko, T. Renger, H.-S. Tan, R. Tempelaar, M. Thorwart, E. Thyrhaug, S. Westenhoff and D. Zigmantas, *Sci. Adv.,* 2020, **6**, eaaz4888.

44 T. Mančal, *Chem. Phys.,* 2020, **532**, 110663–1106693.

45 P. Bhattacharayya and G. R. Fleming, *J. Chem. Phys.,* 2020, **153**, 044119.

46 E. Zerah Harush and Y. Dubi, *Sci. Adv.,* 2021, **7**, eabc4631.

47 N. C. M. Magdaong, H. Jing, J. R. Diers, C. Kirmaier, J. S. Lindsey, D. F. Bocian and D. Holten, *J. Phys. Chem. Lett.,* 2022, **13**, 7906–7910.

48 H. Scheer, H., In *Chlorophylls and Bacteriochlorophylls: Biochemistry, Biophysics, Functions and Applications*, B. Grimm, R. J. Porra, W. Rüdiger and H. Scheer, Eds., Springer, Dordrecht, The Netherlands, 2006, pp 1−26

49 M. Kobayashi, M. Akiyama, H. Kano and H. Kise, In *Chlorophylls and Bacteriochlorophylls. Biochemistry, Biophysics, Functions and Applications*, B. Grimm, R. J. Porra, W. Rüdiger and H. Scheer, Eds., Springer, Dordrecht, The Netherlands, 2006, pp 79–94.

50 S. Zhang, H.-J. Kim, Q. Tang, E. Yang, D. F. Bocian, D. Holten and J. S. Lindsey, *New J. Chem.,* 2016, **40**, 5942–5956.

51 J. S. Lindsey, *Chem. Rev.,* 2015, **115**, 6534–6620.

52 H. Fujita, H. Jing, M. Krayer, S. Allu, G. Veeraraghavaiah, Z. Wu, J. Jiang, J. R. Diers, N. C. M. Magdaong, A. K. Mandal, A. Roy, D. M. Niedzwiedzki, C. Kirmaier, D. F. Bocian, D. Holten and J. S. Lindsey, *New J. Chem*., 2019, **43**, 7209–7232.

53 M. Taniguchi, D. L. Cramer, A. D. Bhise, H. L. Kee, D. F. Bocian, D. Holten and J. S. Lindsey, *New J. Chem.,* 2008, **32**, 947–958.

54 A. Dreuw and M. Head-Gordon, *J. Am. Chem. Soc.*, **2004**, *126*, 4007−4016.

55 N. N. Esemoto, Z. Yu, L. Wiratan, A. Satraitis and M. Ptaszek, *Org. Lett.,* 2016, **18**, 4590−4593.

56 H. Aksu, B. Maiti, M. Ptaszek and B. D. Dunietz, *J. Chem. Phys.,* 2020, **153**, 134111.

57 Z. Yu, B. Uthe, R. Gelfand, M. Pelton and M. Ptaszek, *J. Porphyrins Phthalocyanines,* 2021, **25**, 724–733.

58 J. S. Lindsey, O. Mass and C.-Y. Chen, *New J. Chem*., 2011, **35***,* 511–516.

59 H. Jing, J. Rong, M. Taniguchi and J. S. Lindsey, *Coord. Chem. Rev.,* 2022, **456**, 214278.

60 D. Fan, M. Taniguchi and J. S. Lindsey, *J. Org. Chem.,* 2007, **72**, 5350–5357.

61 H. Jing, P. Wang, B. Chen, J. Jiang, P. Vairaprakash, S. Liu, J. Rong, C.-Y. Chen, P. Nalaoh and J. S. Lindsey, *New J. Chem*., 2022, **46**, 5534–5555.

62 H. Jing, S. Liu, J. Jiang, V.-P. Tran, J. Rong, P. Wang and J. S. Lindsey, *New. J. Chem*., 2022, **46**, 5556–5572.

63 K. E. Borbas, C. Ruzié and J. S. Lindsey, *Org. Lett*., 2008, **10**, 1931–1934.

64 S. Chakraborty, H.-C. You, C.-K. Huang, B.-Z. Lin, C.-L. Wang, M.-C. Tsai, C.-L. Liu and C.-Y. Lin, *J. Phys. Chem. C*, 2017, **121**, 7081–7087. Correction: S. Chakraborty, H.-C. You, C.-K. Huang, B.-Z. Lin, C.-L. Wang, M.-C. Tsai, C.-L. Liu and C.-Y. Lin, *J. Phys. Chem. C*, 2020, **124**, 2728.

65 H.-J. Kim and J. S. Lindsey, *J. Org. Chem.,* 2005, **70**, 5475–5486.

66 R. Chinchilla and C. Nájera, *Chem. Rev.,* 2007, **107**, 874–922.

67 R. W. Wagner, Y. Ciringh, C. Clausen and J. S. Lindsey, *Chem. Mater.,* 1999, **11**, 2974–2983.

68 S. I. Yang, J. Li, H. S. Cho, D. Kim, D. F. Bocian, D. Holten and J. S. Lindsey, *J. Mater. Chem.,* 2000, **10**, 283–296.

69 K.-Y. Tomizaki, A. B. Lysenko, M. Taniguchi and J. S. Lindsey, *Tetrahedron, 2004*, **60**, 2011–2023.

70 E. Hindin, C. Kirmaier, J. R. Diers, K.-Y. Tomizaki, M. Taniguchi, J. S. Lindsey, D. F. Bocian and D. Holten, *J. Phys. Chem. B,* 2004, **108**, 8190–8200.

71 M. Taniguchi, H. Du and J. S. Lindsey, *Photochem. Photobiol.,* 2018, **94**, 277–289.

72 R. S. Knox and H. van Amerongen, *J. Phys. Chem. B*, 2002, **106**, 5289–5293.

73 M. Taniguchi, J. S. Lindsey, D. F. Bocian and D. Holten, *J. Photochem. Photobiol. C: Photochem. Rev.,* 2021, **46**, 100401.

74 R. E. Dale and J. Eisinger, *Biopolymers*, 1974, **13**, 1573–1605.

75 R. R. Birge, D. F. Bocian and L. M. Hubbard, *J. Am. Chem. Soc.*, 1982, **104**, 1196–1207.

76 J. C. Chang, *J. Chem. Phys.,* 1977, **67**, 3901–3909.

77 B. P. Krueger, G. D. Scholes and G. R. Fleming, *J. Phys. Chem. B*, 1998, **102**, 5378–5386.

78 H. S. Kang, N. N. Esemoto, J. R. Diers, D. M. Niedzwiedzki, J. A. Greco, J. Akhigbe, Z. Yu, C. Pancholi, G. V. Bhagavathy, J. K. Nguyen, C. Kirmaier, R. R. Birge, M. Ptaszek, D. Holten and D. F. Bocian, *J. Phys. Chem. A,* 2016, **120**, 379–385.

79 H. S. Kang, A. Satraitis, A. Meares, G. V. Bhagavathy, J. R. Diers, D. M. Niedzwiedzki, C. Kirmaier, M. Ptaszek, D. F. Bocian and D. Holten, *J. Porphyrins Phthalocyanines,* 2021, **25**, 639–663.

80 A. Roy, J. R. Diers, D. M. Niedzwiedzki, A. Meares, Z. Yu, G. V. Bhagavathy, A. Satraitis, C. Kirmaier, M. Ptaszek, D. F. Bocian and D. Holten, *J. Phys. Chem. A,* 2022, **126**, 5107–5125.

81 B. Birks, *Photophysics of Aromatic Molecules,* Wiley Interscience, New York, 1970.

82 R. C. Hilborn, *Am. J. Phys.*, 1982, **50**, 982–986.

83 M. Gouterman, *J. Chem. Phys.,* 1959*,* **30**, 1139−1161.

84 M. Gouterman, *J. Mol. Spectrosc.,* 1961, **6***,* 138−163.

85 M. Gouterman, G. H. Wagnière and L. C. Snyder, *J. Mol. Spectrosc.,* 1963, **11**, 108–127.

86 M. Gouterman, In *The Porphyrins*, D. Dolphin, Ed., Academic Press, New York, 1978, Vol. 3, pp 1−165.

87 R. L. Martin, *J. Chem. Phys.,* 2003, **118**, 4775–4777.